NEUTRON POWDER PATTERN ANALYSIS OF HYDROTHERMALLY DEUTERATED KAOLINITE

A THESIS

Presented to

The Faculty of the Graduate Division

by

Glenn R. Wienkoop

In Partial Fulfillment

of the Requirements for the Degree

Master of Science in Ceramic Engineering

Georgia Institute of Technology

June, 1971

NEUTRON POWDER PATTERN ANALYSIS OF HYDROTHERMALLY

DEUTERATED KAOLINITE

Approved:

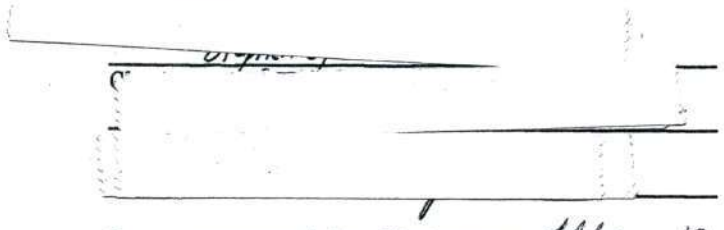

Date approved by Chairman: May 12, 1971

In presenting the dissertation as a partial fulfillment of the requirements for an advanced degree from the Georgia Institute of Technology, I agree that the Library of the Institute shall make it available for inspection and circulation in accordance with its regulations governing materials of this type. I agree that permission to copy from, or to publish from, this dissertation may be granted by the professor under whose direction it was written, or, in his absence, by the Dean of the Graduate Division when such copying or publication is solely for scholarly purposes and does not involve potential financial gain. It is understood that any copying from, or publication of, this dissertation which involves potential financial gain will not be allowed without written permission.

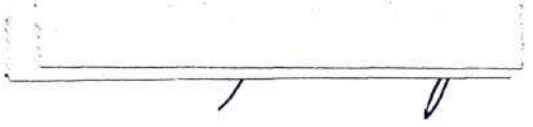

7/25/68

ACKNOWLEDGMENTS

I would like to thank Dr. Stephen Spooner, my principal advisor, for his enthusiasm and constructive guidance.

I would also like to express my appreciation to Thomas H. B. Sanders for writing the necessary computer programs and acting as consultant.

I am indebted to Dr. R. J. Gerdes and Dr. R. A. Young of the Crystal Physics Branch of the Engineering Experiment Station for the use of their laboratory facilities.

I want to thank Dr. Lane Mitchell and Dr. A. T. Chapman for their participation as members of my thesis advisory committee.

The use of the Georgia Tech Research Reactor Facility and help from the staff are gratefully acknowledged.

Lastly, I would like to thank Dr. W. E. Moody for helping to initiate this investigation, and my fiancee and parents for their encouragement.

TABLE OF CONTENTS

LIST OF TABLES

LIST OF TABLES (Concluded)

LIST OF FIGURES

LIST OF FIGURES (Concluded)

SUMMARY

The investigation of a hydrothermally deuterated kaolinite was made. The reconstituted material was found to be similar to normal kaolinite when differential thermal analysis, thermogravimetric analysis, electron microscopy, and x-ray diffraction were used for characterization. In general the analyses revealed that the final reconstituted material was not as well crystallized as the initial kaolinite.

Neutron powder diffraction confirmed the apparent decrease in crystallinity and the analysis of the diffuse background provided an absolute measure of the remaining hydrogen content. A structure analysis indicated that deuterium atoms did not occupy the same coordinates as proposed hydrogens in kaolinite but were found to be the following:

Atom	x	y	z
D_1	.595	.000	.770
D_2	.095	.167	.770
D_3	.595	.333	.770
D_4	.543	.481	.150

Coordinates indicated upper oxygen-deuterium (OD) bonds were inclined away from the c-axis pointing away from Al cations and the lower OD bond pointed down parallel to the c-axis into the vacant octahedral position within the Si-O tetrahedron net. OD bond lengths were longer than oxygen-hydrogen (OH) bond lengths in kaolinite. Examination of the neutron

diffraction pattern indicated that a high probability of nb/3 layer shifting resulted from hydrothermal reconstitution.

CHAPTER I

INTRODUCTION

The structure of kaolinite, not including hydrogens, has been determined using x-ray and electron diffraction. In recent times, neutron diffraction has been applied to structures where hydrogen positions are of primary importance. The reason for using neutron diffraction for hydrogenous compounds can be illustrated by considering the difference between neutron scattering and other forms of scattering. X-rays and electrons are primarily scattered by atomic electrons and consequently the amount of scattering is proportional to the number of electrons. Thus, there is a linear increase of scattering amplitude with atomic number and light elements like hydrogen will not have appreciable scattering amplitudes. In contrast, neutrons are scattered by atomic nuclei and scattering properties are related to nuclear scattering and absorption cross sections. As a result, the scattering amplitude of hydrogen is comparable with that of higher atomic number elements. In addition to considering the coherent scattering cross section, giving rise to structure diffraction effects, and the absorption cross section, related to neutron capture, the effect of neutron incoherent scattering must be examined. Neutron incoherent scattering results from the interaction of neutron and nuclear spins. In the case of kaolinite, structural hydrogens possess nuclei with randomly oriented spins which interact with the neutron spin of ($\pm$ 1/2) to modify

scattering and produce a large diffuse background. This large incoherent background reduces the signal-to-noise ratio diminishing the effectiveness of neutron diffraction. This diffuse background can be largely eliminated through the substitution of deuterium for hydrogen, since the scattering cross section for deuterium is almost completely coherent. Substitution of this isotope would also help substantiate the replaced hydrogen positions due to the large difference in coherent scattering cross sections between hydrogen and deuterium.

Substitution of deuterium for hydrogen in kaolinite has been accomplished by the expansion of kaolinite with potassium acetate and treatment with D_2O vapor or by hydrothermal reconstitution techniques. In general, hydrothermal deuteration has generally been the most accepted method since it allows the largest amount of replacement.

The first detailed investigation of the hydrothermal treatment of kaolinite was performed by Roy and Brindley (1). The resynthesis process was outlined as consisting of a primary dehydration step of heating the kaolin group minerals around 550° to 650°C resulting in the formation of characteristic amorphous meta phases. Subsequent hydrothermal treatment of kaolinite, dickite, nacrite, and halloysite meta phases indicated that meta phases did not revert to initial phases but to a close approximation of kaolinite. Meta kaolinite showed a marked transformation back to kaolinite with the early development of basal reflections and restoration of three-dimensional order after hydrothermal treatment at 370°C and 20,000 psi. The apparent failure of the other meta phases to revert to their initial phases was evidence of interlayer bond rupturing and consequent

layer stacking disorders and perhaps rupturing within the plane of the sheets.

Application of hydrothermal treatment of kaolin minerals has been made to deuterate samples for investigation by infrared spectroscopy. Previous to this technique studies attempted to correlate the OH-bond stretching frequencies of kaolinite to corresponding OH lattice sites of an ideal kaolinite structural model. This approach was hazardous because the structure of kaolinite cannot be studied by single crystal methods and consequently cannot be refined beyond a given point. Selective hydrothermal deuteration produced frequency shifts which could be correlated to structural properties. Early investigations were directed toward identifying frequencies with given OH sites, based on perturbations caused by OD substitutions. Beyond this point only brief consideration has been given to actual OH bond orientations. Serratossa, Hidalgo, and Vinas (2) reported upper layer OH bonds to be perpendicular to the (001) plane and the lower free hydroxyl groups as having bonds pointed into vacant octahedral sites in the plane common to tetrahedral and octahedral sheets. An infrared investigation of dickite correlated to an x-ray single crystal study indicated that upper OH bonds were directed toward closest neighbors in the adjacent kaolinite layer. Newnham (3) assigned the lower OH group to be a free hydroxyl within the octahedral layer. A recent investigation of deuterated kaolinite by Ledoux (4) indicated that deuteration produced a change with respect to initial OH orientations. The net result was that OD bond orientations formed larger angles with respect to the (001) plane than initial OH bonds. Also, (O-D...O) bond

lengths were found to be longer than (O-H...O) bonds prior to deuteration. Initial OH bond orientations were found to be slightly less than 90° to the (001) plane with lower OH groups pointing into vacant octahedral sites. Unfortunately infrared spectroscopy has only been able to provide relative OH bond orientations and not exact proton locations. A recent neutron diffraction investigation has however led to proposed atomic coordinates for hydrogen in the kaolinite structure.

Sanders (5) in a neutron diffraction powder analysis proposed that upper layer hydrogens were approximately pointed toward nearest neighbor oxygens in the basal plane of the above unit cell. O-H...O bond distances indicated that hydrogen bonding was a primary mechanism in interlayer bonding. Bond lengths for these hydrogens were parallel to the oxygen -- oxygen internuclear distances. The lower hydrogen was located in vacant octahedral sites with a bond direction parallel to the c-axis (see Figure 1). Structural analysis also indicated no tetrahedral rotation and a slight octahedral shift, with some refinement of other atomic coordinates (see Table 1).

Other analyses have presented somewhat different atomic coordinates and proposed different structural modifications involving octahedral layer shifting, tetrahedral rotation, and basal plane buckling but have been unable to propose hydrogen coordinates. Brindley and Robinson (6) refined the first model proposed by Gruner (7) presenting an ideal kaolinite model which illustrated a paired relationship between adjacent oxygens and hydroxyls (see Table 2 and Figure 2). A later investigation by Zvyagin (8) using electron diffraction modified the structure proposed by Brindley

Table 1. Coordinates* for the Structure Proposed by Sanders

Atom	x	y	z
O_3	.500	.000	.000
O_4	.755	.745	.000
O_5	.245	.745	.000
Si_1	.518	.830	.075
Si_2	.518	.170	.075
O_1	.572	.170	.300
O_2	.572	.830	.300
OH_4	.543	.481	.300
Al_1	.729	.997	.452
Al_2	.229	.834	.453
OH_3	.443	.993	.595
OH_2	.923	.840	.593
OH_1	.425	.670	.591
H_1	.461	.000	.723
H_2	.610	.708	.723
H_3	.639	.793	.723
H_4	.543	.481	.165

*Coordinates recomputed on basis of 104° unit cell origin

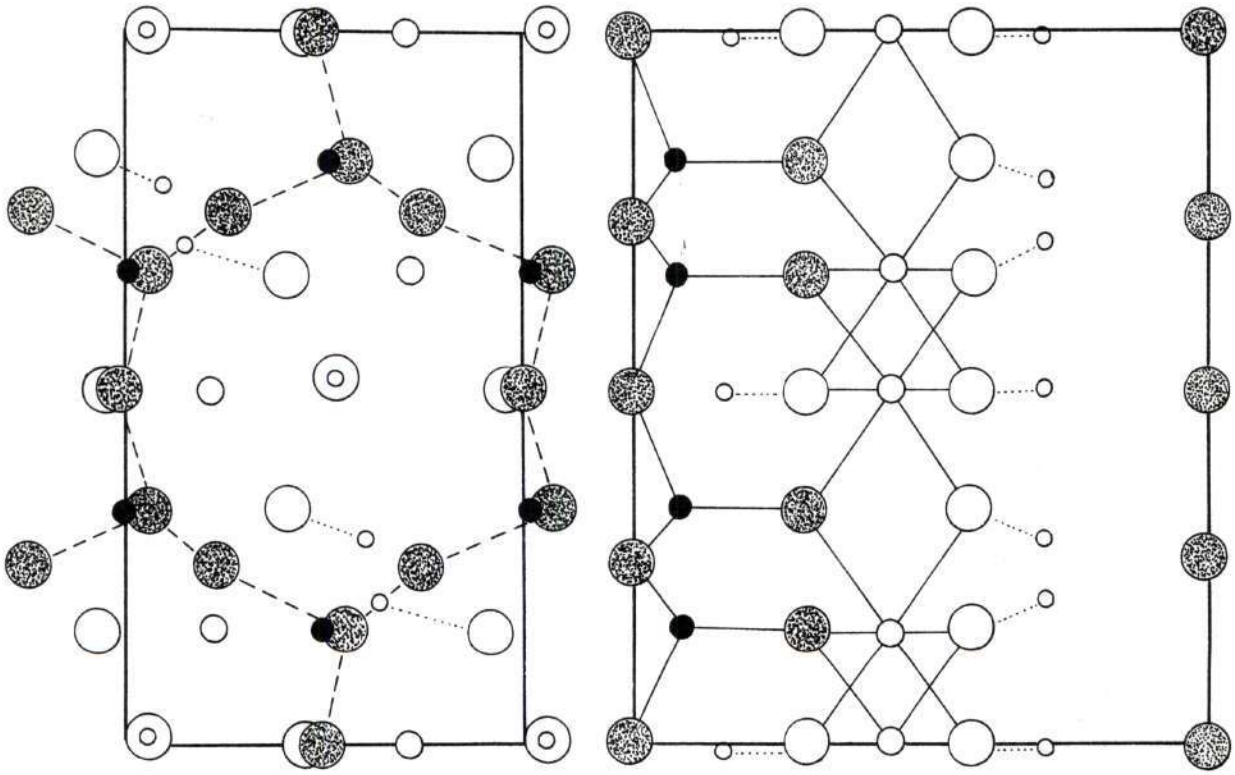

(a) (001) Plane

(b) (100) Plane

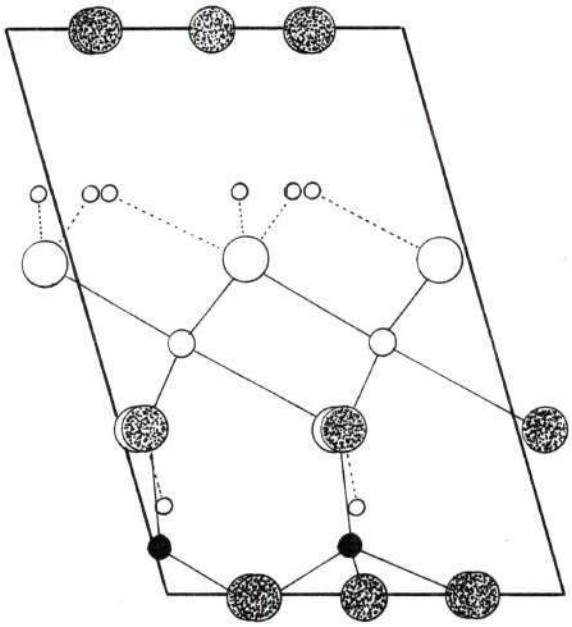

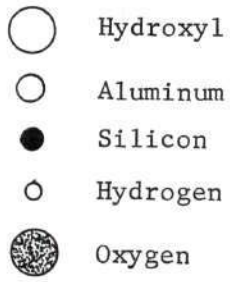

(c) (010) Plane

Figure 1. Sanders' Kaolinite Structure Projected on Various Planes

Table 2. Coordinates* for the Structure Proposed by Brindley and Robinson

Atom	x	y	z
O_3	.500	.000	.000
O_4	.750	.750	.000
O_5	.250	.750	.000
Si_1	.500	.833	.081
Si_2	.500	.167	.081
O_1	.500	.167	.297
O_2	.500	.833	.297
OH_4	.500	.500	.297
Al_1	.667	.000	.444
Al_2	.167	.167	.444
OH_3	.333	.000	.593
OH_2	.833	.833	.593
OH_1	.333	.667	.593

*Coordinates recomputed on basis of 104° unit cell origin

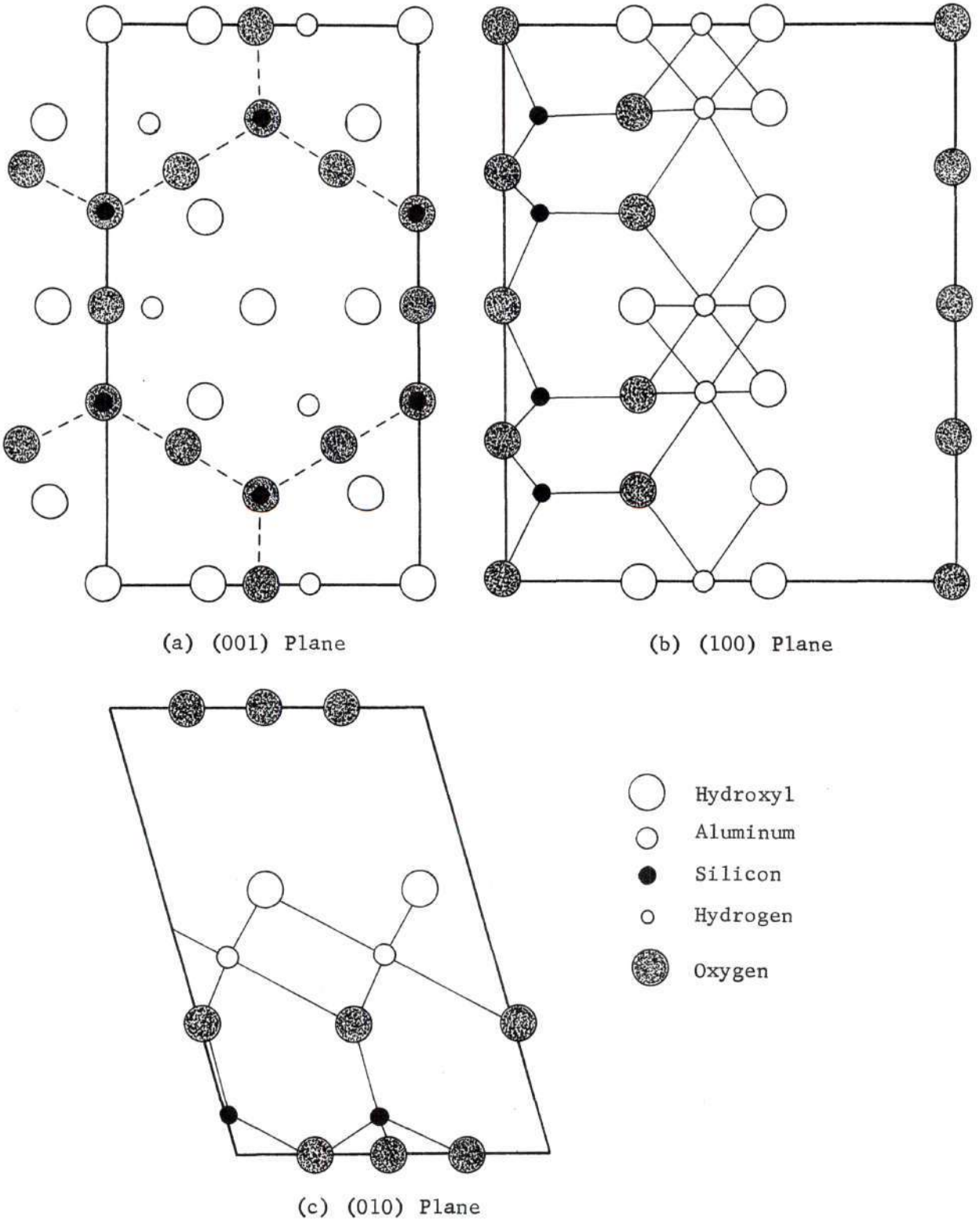

Figure 2. Brindley and Robinson Structure Projected on Various Planes

and Robinson by rotating structural units within the unit cell. Lower and upper bases of octahedrons were concluded to be rotated 3° and 5° respectively, and the bases of the tetrahedrons rotated an average of 20°. The consequence of such rotations shortened common edges of octahedrons, flattened octahedrons, displaced Al atoms toward the lower OH bases, and displaced Si atoms toward the tetrahedron bases. This structure was essentially confirmed by an x-ray single crystal analysis made by Drits and Kashaev (9). The analysis reported a 21° tetrahedron rotation and a 6.5° and 4° rotation of the lower and upper octahedrons, respectively (see Table 3 and Figure 3). The most current x-ray diffraction analysis of the kaolinite structure made by Newnham (10) suggested that silica tetrahedrons were rotated by 7.5° in opposite directions and that the silica sheet was puckered in the basal oxygen plane. The large structural modifications proposed by Zvyagin, Drits and Kashaev, and Newnham suggest that their experimental investigations were performed on poorly crystallized kaolinite varieties with structural distortions. The similarity of the Brindley and Robinson model and the model proposed by Sanders suggests that well crystallized kaolinites were investigated in both cases.

It was the objective of this research to continue Sanders' investigation and locate hydrogen positions more precisely through neutron diffraction analysis of a hydrothermally reconstituted deuterated kaolinite. Detailed characterization of the deuterated kaolinite was done using x-ray diffraction, thermogravimetric analysis, differential thermal analysis, and scanning electron microscopy. Results were compared to

Table 3. Coordinates* for the Structure Proposed by Drits and Kashaev

Atom	x	y	z
O_3	.500	.000	.000
O_4	.817	.777	.000
O_5	.321	.715	.000
Si_1	.509	.167	.073
Si_2	.509	.835	.070
O_1	.463	.140	.300
O_2	.399	.839	.298
OH_4	.957	.019	.300
Al_1	.211	.007	.452
Al_2	.707	.165	.453
OH_3	.487	.015	.595
OH_2	.987	.155	.593
OH_1	.025	.827	.591

*Coordinates recomputed on basis of 104° unit cell origin

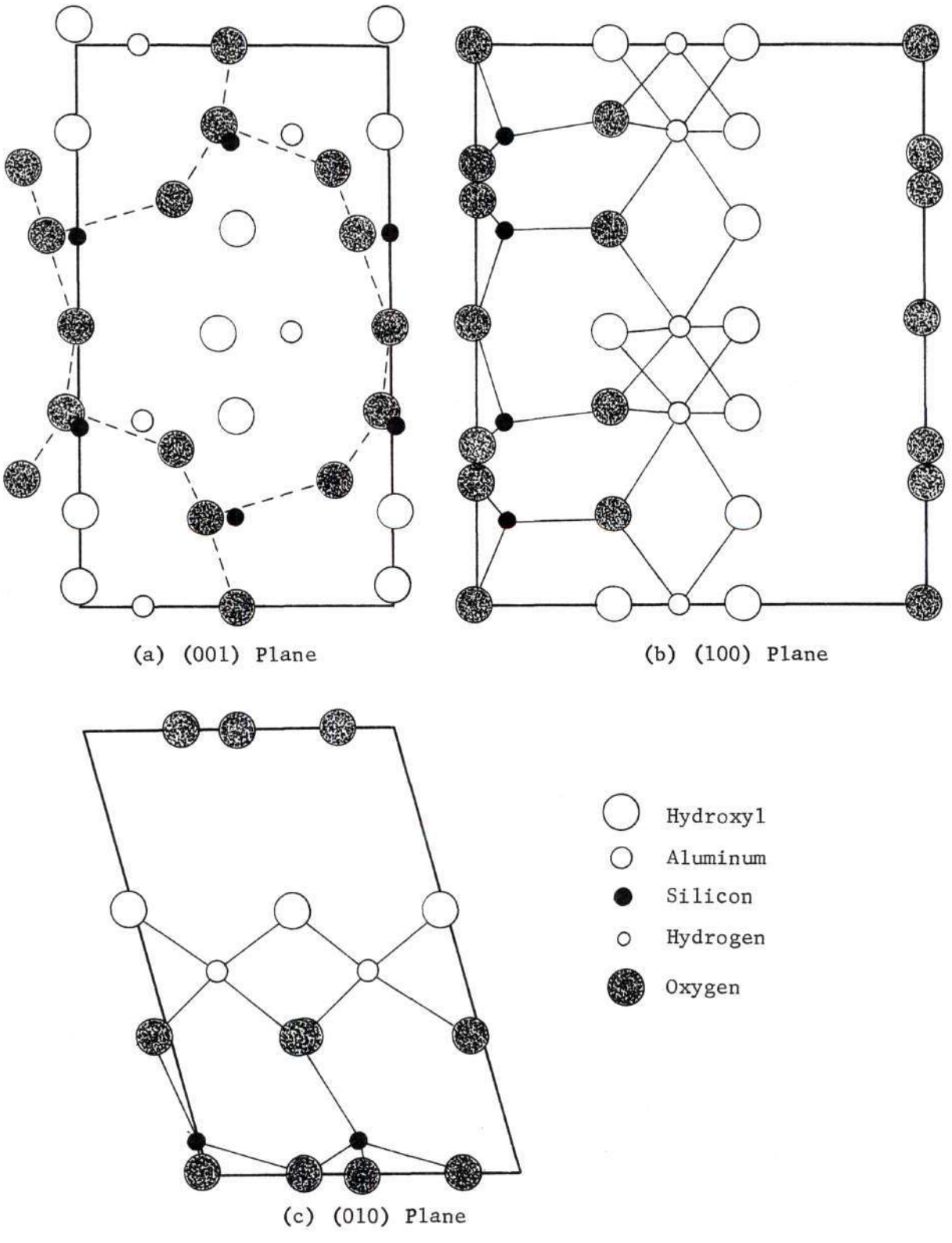

Figure 3. Drits and Kashaev Structure Projected on Various Planes

similar examinations made on the well crystallized kaolinite prior to dehydration and hydrothermal deuteration. Neutron diffraction data were taken for the structural analysis and the diffuse background scattering in the pattern was examined for residual hydrogen content. The structure analysis was made by computer generation of a neutron diffraction pattern which best fit the experimental pattern.

CHAPTER II

EXPERIMENTAL PROCEDURE

Sample Preparation

The well crystallized kaolinite sample used in Sanders (5) research, obtained from Twiggs County, Georgia, was used for this investigation. In preparation for hydrothermal treatment, the kaolinite sample was dehydrated by heating to 800°C at 15°C/min. The dehydrated sample was quenched in 99 percent pure D_2O and adjusted to give a 40 percent solids mixture content. The D_2O-meta kaolinite mixture was sealed in a platinum-lined, MRA-138S reaction vessel designed by Tem-Pres Corporation. Initial pressurization of the vessel to 10,000 psi was produced from a gas operated intensifier on a HR-1B Tem-Pres hydrothermal research unit. Final pressurization was achieved through heating the reaction vessel to 350°C. Hydrothermal conditions of 350°C and 37,500 psi were maintained for 20 days to obtain a deuterated and reconstituted kaolinite.

Sample Characterization

The deuterated kaolinite obtained from hydrothermal reconstitution was characterized using x-ray fluorescence spectroscopy, neutron activation, scanning electron microscopy, differential thermal analysis, thermogravimetric analysis, and x-ray diffraction. Impurity content, morphology, thermal characteristics, and x-ray diffraction information were correlated to an identical characterization of the kaolinite before deuteration.

Impurity analysis of kaolinite and deuterated kaolinite was made with a Norelco x-ray spectrograph. X-ray spectrograph measurements were made using a tungsten x-ray source operated at 45 kv and 45 ma. LiF and EDDT analyzing crystals were used with scintillation and gas flow counting modes, respectively, to enable elemental analysis from atomic number 13 to atomic number 40. Qualitative impurity content was determined by $1/4°/min.$ 2θ scans and quantitative results were obtained by comparison of peak intensities and fixed time counting measurements with results recorded from a National Bureau of Standards clay. Neutron activation analysis was performed to confirm x-ray fluorescence results. Samples were prepared for γ-ray spectrograph analysis by irradiation in flux conditions of 1×10^{13} n $cm^{-2} sec^{-1}$ at the Georgia Tech Research Reactor. Kaolinite specimens were counted at a mean distance of 2 cm from the face of a 3 in. x 3 in. NaI(Tl) detector. The amount of elemental impurity was obtained by multiplying the weight of an elemental standard by the ratio of observed sample counting rate to standard counting rate.

The morphology of the hydrothermally deuterated kaolinite was investigated using a Stereoscan Mark IIA Scanning Electron Microscope developed by Cambridge Instrument Company. Specimens were prepared by depositing an ethanol and deuterated kaolinite mixture on an .8 cm aluminum disk and vapor depositing a gold-palladium alloy on the air dried sample. A 30 kv potential was used to accelerate electrons onto the specimen to produce a secondary beam characteristic of the specimen topography. The secondary beam was displayed for photographic recording using a high resolution cathode ray tube.

Kaolinite and deuterated kaolinite specimens were also characterized on the basis of differential thermal and thermogravimetric analyses. Differential thermal analysis (DTA) was used to investigate endothermic and exothermic reactions as a function of temperature. Observations were made using a R. L. Stone "Controlled Environment System" with a SH-9A powder sample holder and a dynamic air atmosphere. 25 mg samples were heated from ambient to 1100°C at 15°C/min to observe major energy changes. A calcined alumina standard was used as a reference material and as an unknown to measure possible thermocouple drift. To observe weight loss as a function of temperature a thermogravimetric analysis (TGA) was made using a Cahn R. G. Electrobalance coupled to a KA-H Recorder-Controller. 10 mg samples were heated at 15°C/min from room temperature to 900°C in an evacuated sample containment vessel to eliminate air drift and erroneous weight gains due to sample volatilization. Results were recorded on a strip chart calibrated to allow a 2 mg full scale deflection.

The structural characterization of kaolinite and deuterated kaolinite by x-ray diffraction included diffractometer scans to establish reconstitution of the deuterated kaolinite and to determine crystallite size. A lattice parameter determination was also made for the deuterated kaolinite to permit comparison to parameters obtained by Sanders (5) on the untreated kaolinite. X-ray diffractometer scans were made using a Norelco diffractometer with a copper target x-ray tube and a nickel filter operating at 40 kv and 25 ma. The pulse height analyzer was set at 90 percent with a time constant of four and a scan rate of 1/8°/min. The

crystallite size determination was made by examining the broadening of several peaks through the measurement of full width at half maximum and correction for doublet separation. Comparison of corrected widths to a plot of instrumental breadth versus 2θ, obtained from a strain free silicon wafer (crystallite size greater than 10,000Å), allowed the calculation of crystallite size by the method outlined by Klug and Alexander (11). The mean crystallite size, D, was calculated by the Scherrer equation:

$$D = \frac{K\lambda}{\beta \cos \theta} \qquad (1)$$

A calculation of equivalent spherical crystallite size was made by extrapolating a plot of $\beta \cos \theta$ versus $\sin \theta$ to 0°. Lattice parameter determinations were made using a 114.6 mm Hull-Debye-Scherrer camera employing the Straumanis film loading technique. Deuterated kaolinite was mixed with a 15 percent by weight NaCl internal standard and exposed for various times using CuK_{α} radiation. Lattice parameter calculations were performed using a FORTRAN program run on the Univac 1108 computer (5).

Powder Neutron Diffraction

Neutron diffraction analysis of deuterated kaolinite was made using a neutron diffractometer at the Georgia Tech Research Reactor facility. A beam of thermal neutrons was monochromated to a wavelength of 1.54Å by diffraction from the (200) plane of a large copper single crystal. Soller slits with 30 and 15 minutes-of-arc nominal resolution were

used to collimate the beam between the scattering sample and a boron fluoride detector, respectively. A relatively short counting time pattern was used to determine absolute hydrogen content and a second longer counting time pattern with improved statistical precision was used for a structure analysis of deuterated kaolinite.

Hydrogen Content Analysis

A neutron diffraction pattern was obtained by stepping in .1 degree intervals from 10°-70° 2θ using fixed time counting of 2 minutes per point. The pattern allowed the selection of a point relatively free from coherent scattering contributions at 15° 2θ. The diffuse background at this point in terms of neutron counts per unit time can be represented by the following equation:

$$\text{Counts/time} = K \left[\sum N_i \sigma_i / 4\pi + P_{ms} \right] A + B \qquad (2)$$

where the summation is made over all the nuclei in the specimen, N_i is the number of each type of nuclei, $\sigma_i/4\pi$ is the incoherent scattering cross section per steradian, K is the instrumental constant, P_{ms} is the multiple scattering contribution, A is the adsorption factor, and B is an instrumental background counting rate (12).

In order that the multiple scattering contribution can be calculated by the Blech and Averbach method (13), the relative transmission of the neutron beam at $2\theta = 0^{\circ}$ must be measured. This was accomplished by collimating the neutron beam through a 4 mm tube embedded in a boron

carbide block incident on the .75 in. diameter, 2.0 in. high aluminum sample container. Incident and transmitted intensities, I_o and I_t, were measured with and without a cadmium sheet obstructing the beam to eliminate fast neutron contributions. Relative transmission was calculated by the following expression:

$$T = \frac{I_t - I_t^{Cd}}{I_o - I_o^{Cd}} \tag{3}$$

where the Cd superscript refers to cadmium transmission. Using the value for relative transmission, T, and the specimen diameter, D, the attenuation factor A was calculated from the relation

$$T = e^{-AD} \tag{4}$$

The value of A and the ratio of specimen radius to height, R/h, permits the multiple scattering parameter, δ, to be obtained from Blech and Averbach's tables (13). Thus, the ratio of multiple scattering to total scattering was calculated by the formula

$$\frac{\sigma_{ms}}{\sigma_s} = \frac{\delta(\sigma_s/\sigma_T)}{1 - \delta(\sigma_s/\sigma_T)} \tag{5}$$

where σ_{ms} is the multiple scattering cross section, σ_s is the total

scattering cross section, and σ_T is the total scattering cross section plus absorption (see Table 4) (14).

Table 4. Neutron Cross Sections and Scattering Factors for Deuterated Kaolinite Atoms

Atom	b (10^{-12} cm)	σ_{coh} (barns)	σ_{inc} (barns)	σ_a (barns)
Al	.35	1.5	0.0	0.13
Si	.42	2.16	0.04	0.06
O	.577	4.2	0.02	0.0001
D	.650	5.4	2.2	0.0005
H	-.378	1.79	79.71	0.19

The background intensity measured at 15° 2θ was corrected for background and multiple scattering according to these procedures and resultant intensities adjusted to be proportional to the 7.9 grams of deuterated kaolinite in the beam. A similar procedure was performed for V_2O_5 to be used as a standard scatterer to evaluate K in equation (2). After the determination of K, the solution for the number of hydrogen nuclei was possible using the same equation (12).

Powder Diffraction Analysis

Neutron diffraction data were obtained for scattering angles from 10° to 70° with fixed-time counting of 5 minutes and in 0.1° intervals in 2θ. The increased statistical precision in this pattern better allowed structural investigation.

These data were compared with computer generated powder patterns based on selected variations in coordinates for the atoms in the kaolinite unit cell. The principle of the calculation is based on the same gaussian broadening of Bragg peak intensities used in the work of Sanders (5). The Bragg peak intensity for a cylindrical powder specimen is given:

$$P_{hkl} = K \frac{j\ N_c^2\ F_{hkl}^2}{\sin\theta\ \sin 2\theta} \tag{6}$$

where K was a constant diffraction geometry factor, j was the multiplicity, N_c was the number of scattering nuclei per unit cell, and F_{hkl} was the structure factor (14). The structure factor is given:

$$F_{hkl} = \sum_j b_j e^{2\pi i(hu_j + kv_j + lw_j)}\ e^{-B_j(\sin^2\theta/\lambda 2)} \tag{7}$$

where b_j is the neutron scattering amplitude, B_j is the isotropic temperature factor, and u_j, v_j, and w_j are the atomic coordinates. In the kaolinite structure under investigation, there are 17 atoms in the asymmetrical unit cell including four hydrogen (deuterium) atoms. Crystallographic symmetry relations involving C Face-Centering translations are used in the computation to generate the remaining atom coordinates in the unit cell. Isotropic temperature factors were assumed to be zero for all atoms except for deuteriums which were 3.34 (5).

The powder pattern is generated by folding a gaussian broadening function into the Bragg peak intensities according to the integral:

$$I_{powder}(2\theta) = \frac{1}{(4\pi B)^{1/2}} \sum_{hkl} \int_{-\infty}^{\infty} P_{hkl} \exp(2\theta - x)^2/B^2 \, dx \qquad (8)$$

where the summation is taken over values of P_{hkl} that can contribute broadened intensity at 2θ and the integral is evaluated numerically over a range in which the gaussian function is reasonably different from zero. The broadening parameter, B, is a function of instrumental, particle size and nb/3 shifting parameters. Caglioti, Paoletti, and Ricci (15) describe an equation using collimation parameters in Table 5 to evaluate instrumental effects. The Scherrer equation for particle size and a modified form of this relation for faulting effects (16) are used to compute the specimen broadening contributions.

Table 5. Collimator and Monochromator Broadening Parameters

Parameter	Value (degrees)
A_1	0.50
A_2	2.00
A_3	0.25
B_1	0.22

The instrumental broadening parameters A_1, A_2, and A_3 are the horizontal

angular divergences of collimators located within the reactor pile, between the monochromator and the sample, and between the sample and the detector, respectively. The factor B_1 is included in the calculation to compensate for broadening due to the mosaic spread of the monochromating crystal.

Since the incident neutron radiation contains $\lambda/2$ intensity, both λ and $\lambda/2$ diffraction patterns are superimposed. For certain reflections the $\lambda/2$ pattern is comparable to small peak intensities in the λ pattern. Therefore, both λ and $\lambda/2$ patterns were calculated in the manner described above with the ratio of intensities of the two patterns being adjusted by a constant factor.

The powder pattern calculations were performed on the Univac 1108 using a program written by Sanders (5). The program is flow charted in Figure 4 and the data input is summarized as follows:

(a) Lattice parameters,

(b) Possible hkl's and corresponding powder pattern multiplicities,

(c) Number of atoms in the unit cell,

(d) Identification of atoms, their coordinates, neutron scattering factors, and isotropic temperature factors,

(e) Description of applicable translational and rotational symmetry operations,

(f) Wavelength and a $\lambda/2$ pattern intensity factor,

(g) Calculation limits from initial to final 2θ,

(h) Horizontal angular divergences of the collimators and the mosaic spread of the monochromating crystal,

(i) Length of the plot.

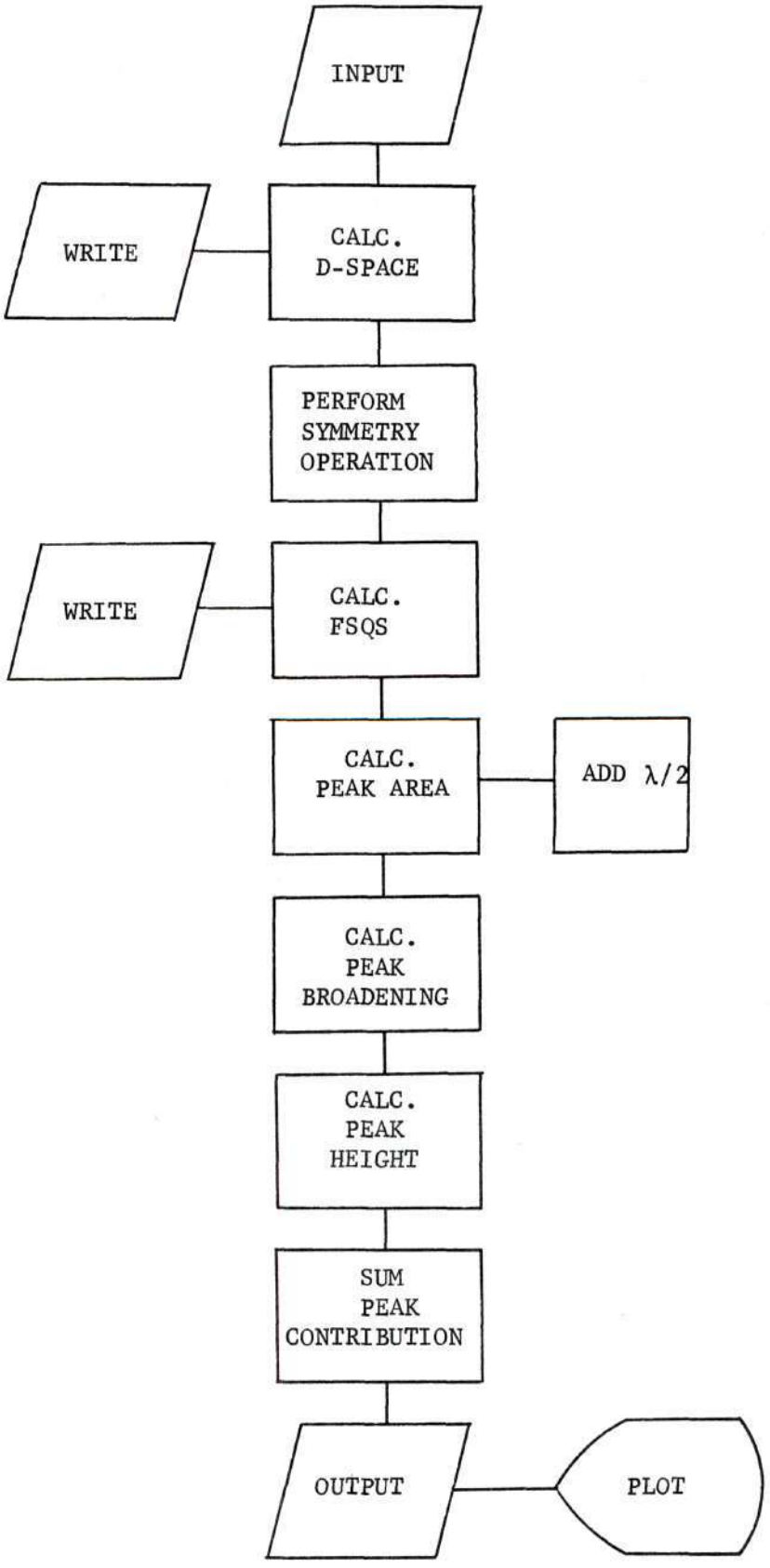

Figure 4. General Computer Flow Diagram for the Calculation of Neutron Diffraction Patterns

CHAPTER III

RESULTS AND DISCUSSION

The available literature indicates that deuterated kaolinite has never been characterized or structurally investigated. Primary studies of this material have been made in infrared spectroscopy under the assumption that properties and structure of the kaolinite have not been altered by deuteration. This research was conducted in part to determine the validity of this assumption and to confirm previously proposed hydrogen positions. Investigation by x-ray diffraction, differential thermal and thermogravimetric analyses, and electron microscopy indicated that kaolinite properties had been slightly altered by hydrothermal deuteration. A powder neutron diffraction analysis confirmed that structural changes had occurred. The advantage of neutron diffraction was that it was more sensitive to the structural changes than x-ray diffraction or any of the other experimental measurements used.

Sample Characterization

Neutron activation and x-ray fluorescence analyses indicated a relatively pure kaolinite with less than 1.4 percent total impurity content. Discrepancy between the results of each analysis technique was probably due to the fact that x-ray fluorescence analysis is largely limited to observing surface rather than bulk impurities. Impurity con-

tent of the deuterated kaolinite was identical with the exception that .05 percent more Co was present due to corrosive attack of the reaction vessel seals (see Table 6).

The scanning electron microscope investigation of deuterated kaolinite morphology indicated disruption of the hexagonal platlet geometry (see Figures 5 and 6). However, the kaolinite stacking characteristic as well as the general hexagonal morphology remained after hydrothermal treatment. The large number of fragmented particles were considered to be a consequence of hydrothermal treatment and evidence of some overall reduction in crystallinity.

A differential thermal analysis of deuterated kaolinite revealed a downward temperature shift of reaction peaks and a decrease in intensity when compared to the original untreated kaolinite (see Figure 7). This was evidence of a slight decrease in structural order resulting from hydrothermal deuteration.

Thermogravimetric analysis revealed similar shaped weight loss curves for kaolinite and deuterated kaolinite (see Figure 8). The kaolinite sample possessed a 14.1 percent weight loss which agreed closely with the calculated theoretical value of 13.95 percent. Examination of the reconstituted sample indicated a 15.3 percent weight loss as compared to a theoretical loss of 15.5 percent for a completely deuterated kaolinite, $Al_2O_3 \cdot 2SiO_2 \cdot 2D_2O$. The .2 percent deviation indicated that the sample was not completely deuterated and the ratio of observed and theoretical weight losses suggested 98 percent deuteration. In the event that

Table 6. Impurity Analysis of Kaolinite

Impurities	X-ray Fluorescence percent	Neutron Activation percent
Titanium	0.850	0.6722
Iron	0.239	0.1898
Potassium	0.170	0.1299
Zirconium	0.080	------
Calcium	0.024	------
Sodium	-----	0.0217
Vanadium	-----	0.0143
Chromium	0.017	0.0090
Manganese	-----	0.0027
Cobalt	-----	0.0004

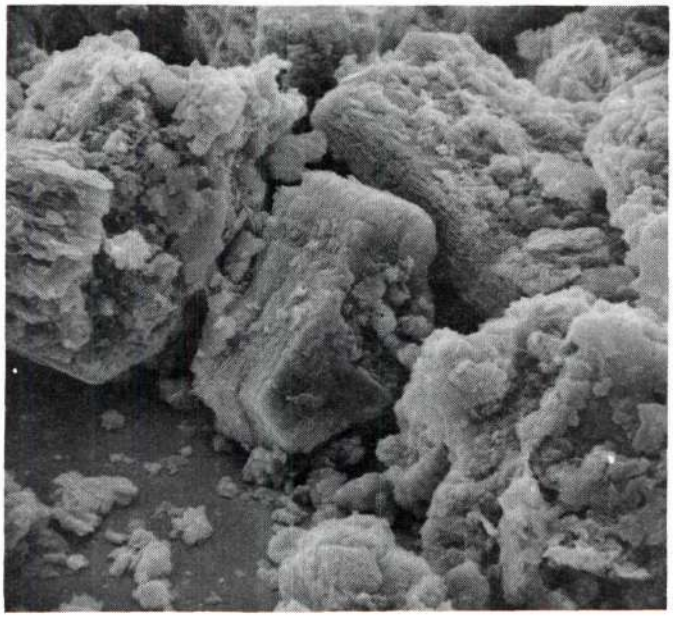

Figure 5. Scanning Electron Micrograph of Deuterated Kaolinite 1090x

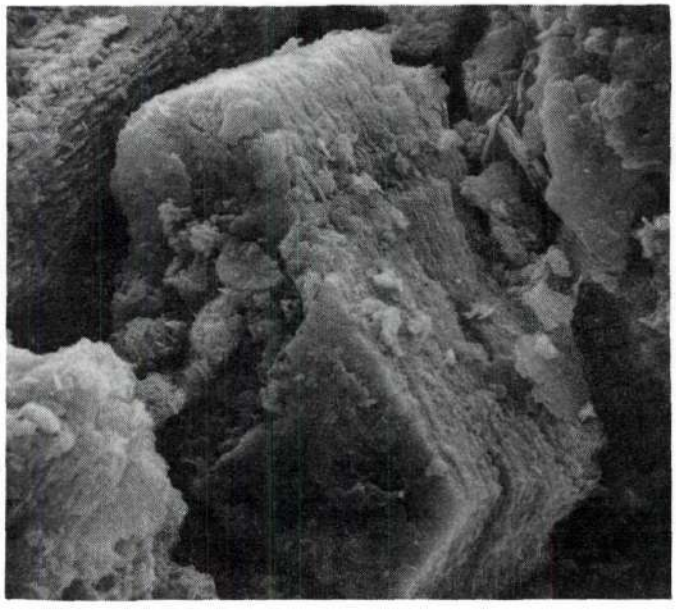

Figure 6. Scanning Electron Micrograph of Deuterated Kaolinite 2180x

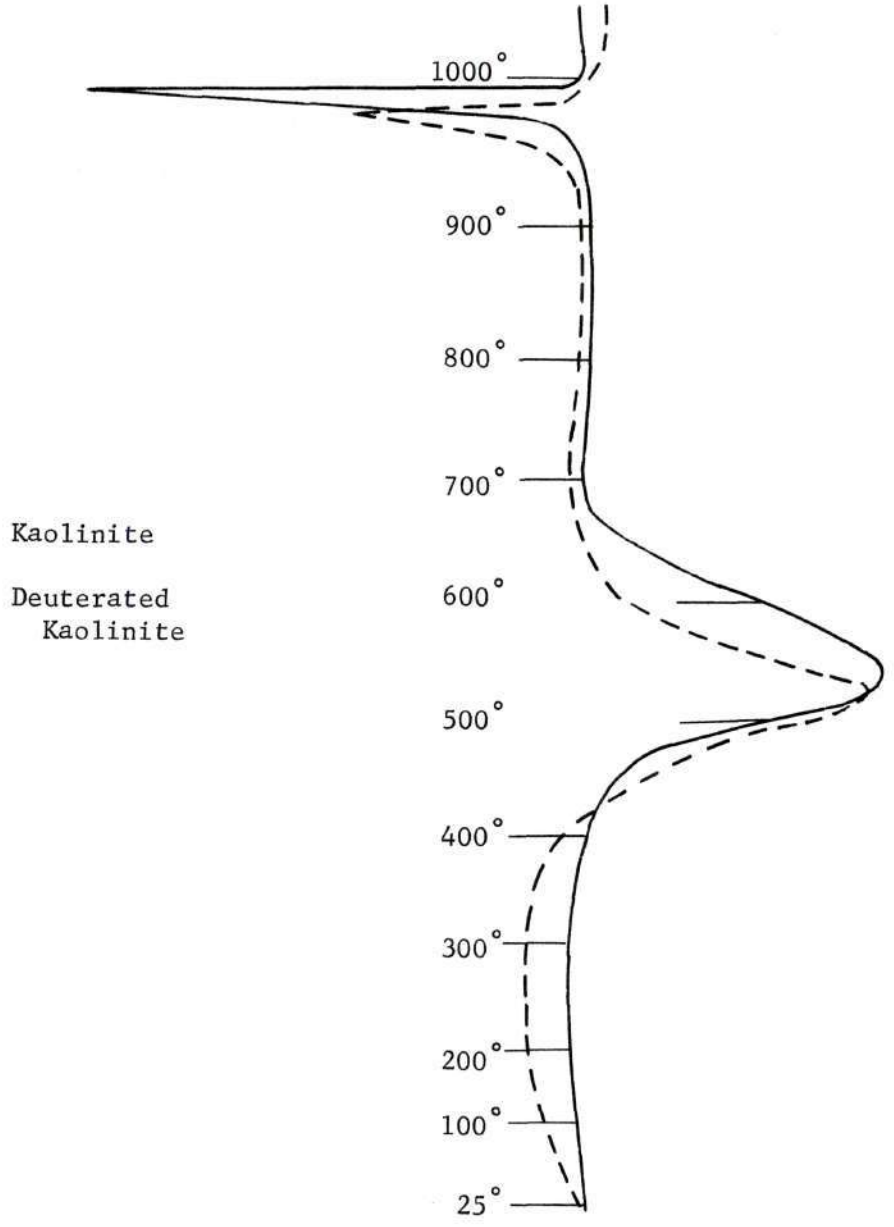

Figure 7. Differential Thermal Analysis Curves for Kaolinite and Deuterated Kaolinite

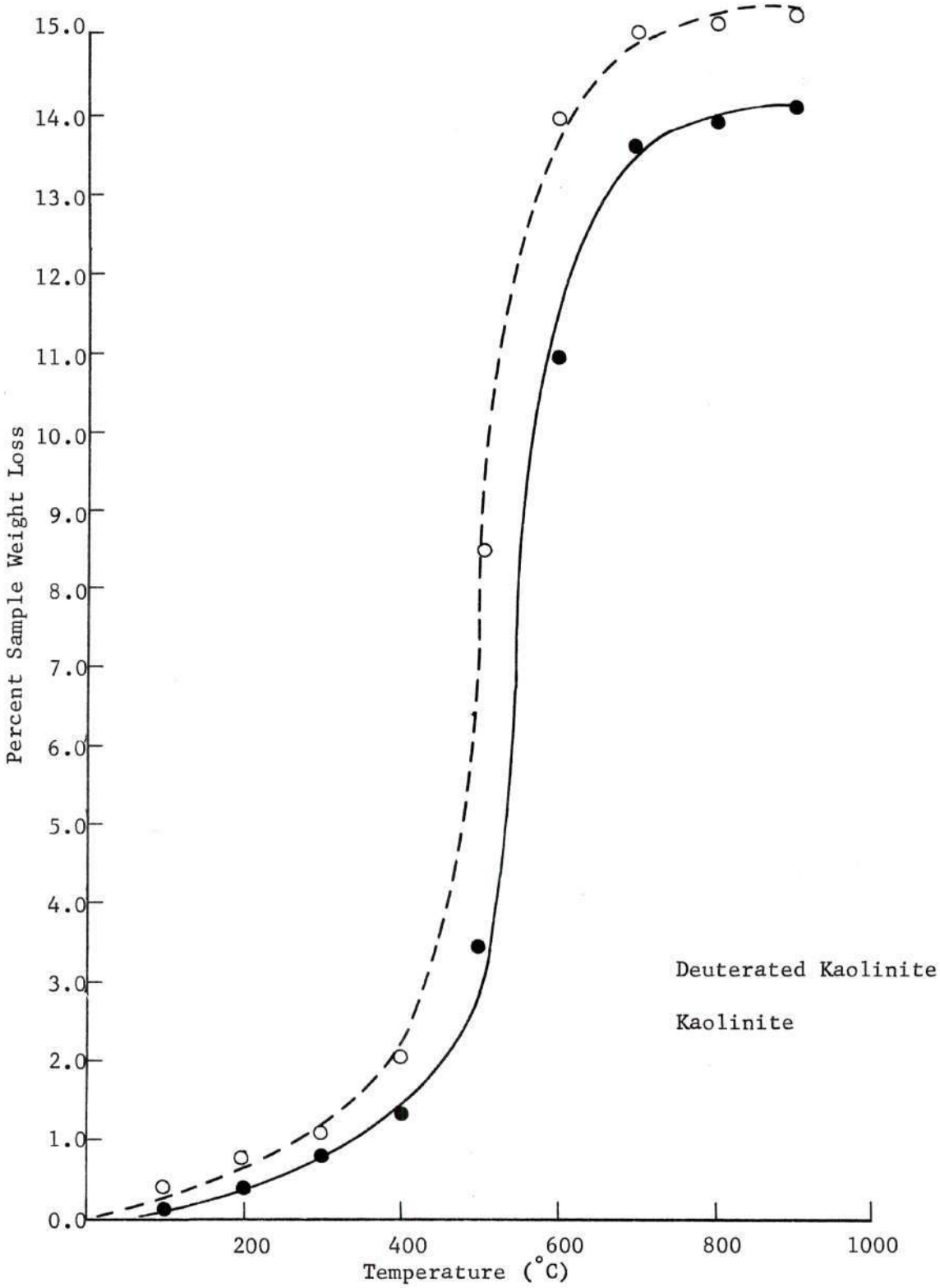

Figure 8. Weight Loss Curves for Deuterated Kaolinite and Kaolinite

all hydrogen had not been removed the total weight loss would be attributed to a combination of D_2O-H_2O dehydration.

X-ray diffraction analysis of deuterated kaolinite consisted of a crystallite size determination and a lattice parameter determination. Diffractometer scans of kaolinite and deuterated kaolinite revealed that the deuterated variety was not as well crystallized and many Bragg peak intensities had been reduced (see Figure 9). It was concluded from this qualitative analysis, that hydrothermal deuteration did reconstitute the amorphous meta kaolinite but only to a close approximation of the initial structural order. Some of the pattern discrepancies could have been accounted for by differences in the relative amounts of preferred orientation. The crystallite size determination indicated that deuterated kaolinite possessed a nearly equivalent spherical crystallite size of 694Å in comparison to kaolinite with 631Å. With this small discrepancy it was assumed that hydrothermal treatment had little effect on crystallite size. Hull-Debye-Scherrer film readings of deuterated kaolinite indicated small variations in d-spacing compared to the original kaolinite. Calculation of lattice parameters by computer program indicated a slight distortion of the kaolinite triclinic unit cell (see Table 7 and Figure 10).

Neutron Diffraction Analysis

Hydrogen Content Analysis

Analysis of the diffuse background of the neutron diffraction pattern allowed the calculation of the number of protons in the deuterated kaolinite sample to be $.54 \times 10^{22}$. Examination of the untreated kaolinite

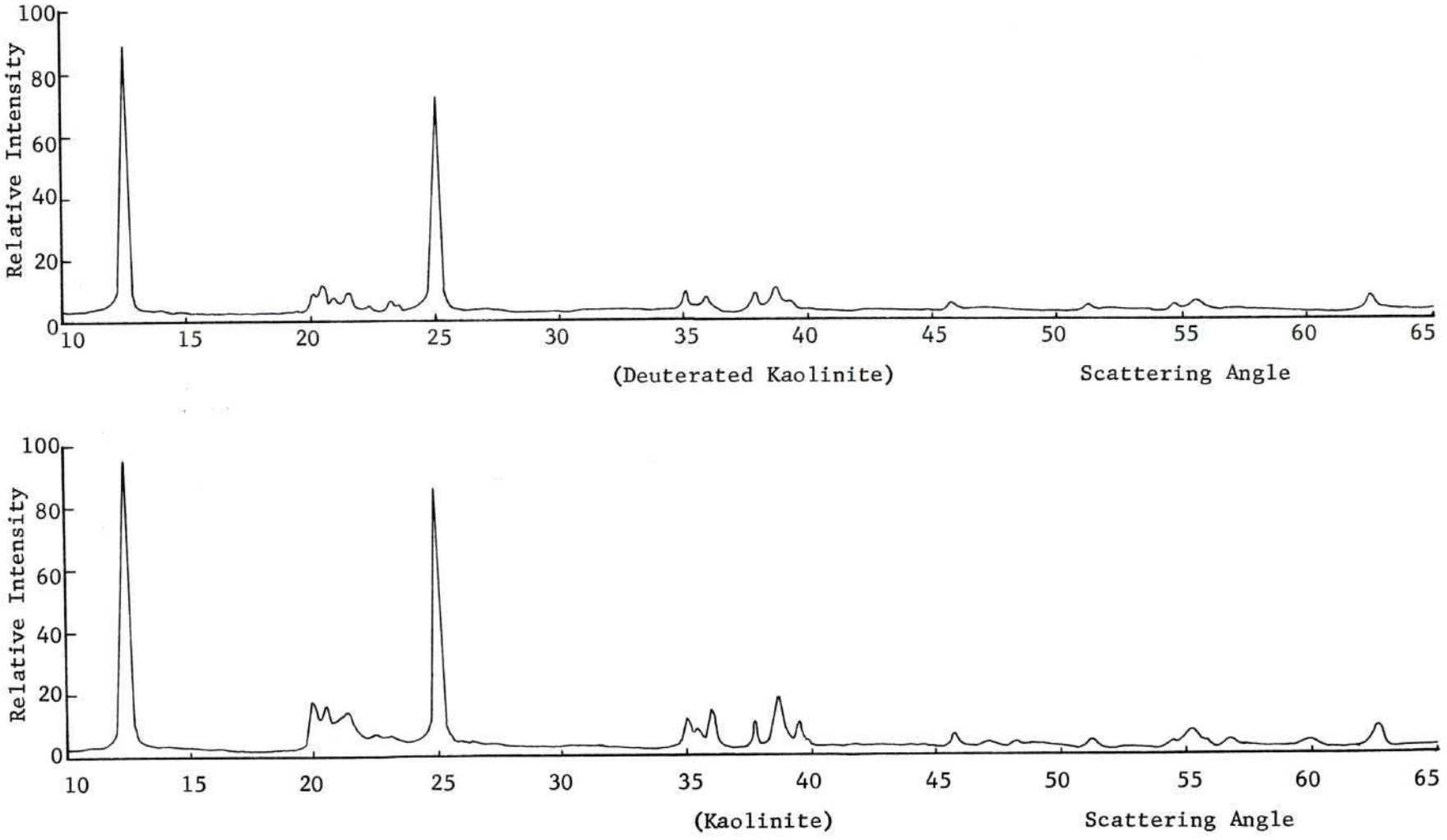

Figure 9. X-ray Diffraction Patterns for Deuterated Kaolinite and Kaolinite

Table 7. Lattice Parameters for Kaolinite and Deuterated Kaolinite

Parameter	Kaolinite	Deuterated Kaolinite
a	5.148 ± .005 Å	5.156 ± .005 Å
b	8.945 ± .005 Å	8.900 ± .005 Å
c	7.386 ± .005 Å	7.378 ± .005 Å
α	91.95 ± .01°	91.95 ± .01°
β	104.22 ± .01°	104.90 ± .01°
γ	90.03 ± .01°	90.02 ± .01°

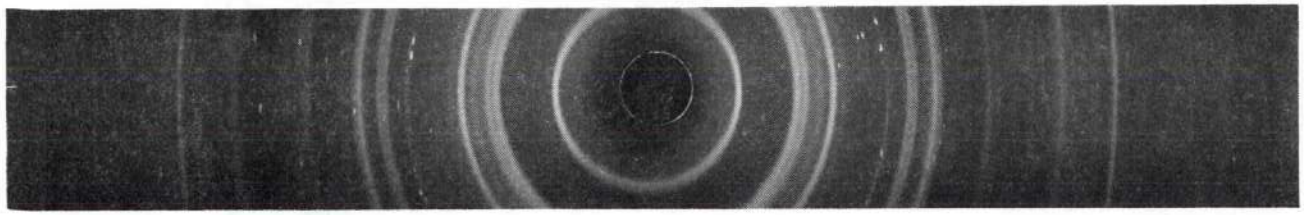

(Deuterated Kaolinite)

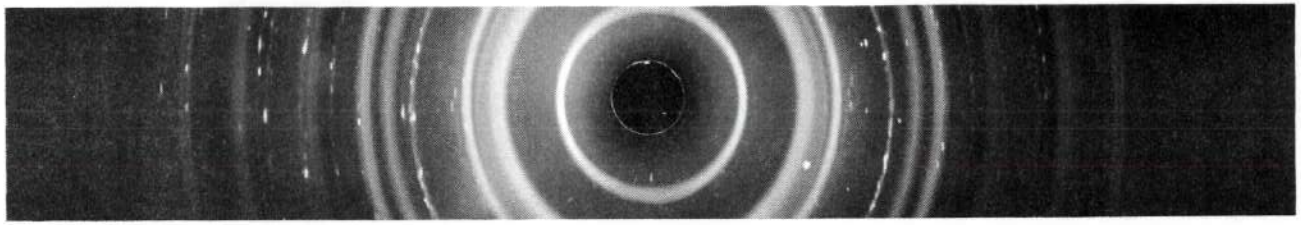

(Kaolinite)

Figure 10. HDS Films for Kaolinite and Deuterated Kaolinite

unit cell, $Al_2O_3 \cdot 2SiO_2 \cdot 2H_2O$, indicated that the 7.9 gram sample would have 7.37×10^{22} protons. The ratio of the two hydrogen contents established that 7 percent of the hydrogen in the unit cell remained after deuteration. Thus, 93 percent deuterium for hydrogen substitution had occurred which can be compared to thermogravimetric results if a modified chemical formula of $Al_2O_3 \cdot 2SiO_2 \cdot 2(2xH + 2yD + 20)$ is considered for the reconstituted unit cell, where x was the decimal fraction of hydrogen remaining and y the decimal fraction of deuterium. According to the neutron diffraction analysis, $x = .07$ and $y = .93$, and with the substitution of these H:D ratios dehydration weight loss from the above chemical formula was 15.4 percent comparing favorably with 15.3 percent recorded by the thermogravimetric analysis.

Neutron Powder Diffraction Pattern

The pattern obtained from the neutron diffraction of deuterated kaolinite was characteristic of a poorly crystallized fireclay kaolinite (see Figure 11). Significant differences existed in the deuterated powder pattern in comparison to a normal kaolinite powder pattern due to the substitution of deuterium for hydrogen. This was an expected effect since deuterium's scattering factor is $.65 \times 10^{-12}$cm in comparison to hydrogen with a scattering factor of $-.378 \times 10^{-12}$cm. The lack of crystallinity was made evident by the peak width broadening and intensity decreases of Bragg peaks. Peak shapes in general were broad but with no apparent two-dimensional effects. Two-dimensional effects tend to skew hk reflections toward high angles and leave 001 type peaks sharp and unaffected for kaolinite layered materials. Another predominant feature

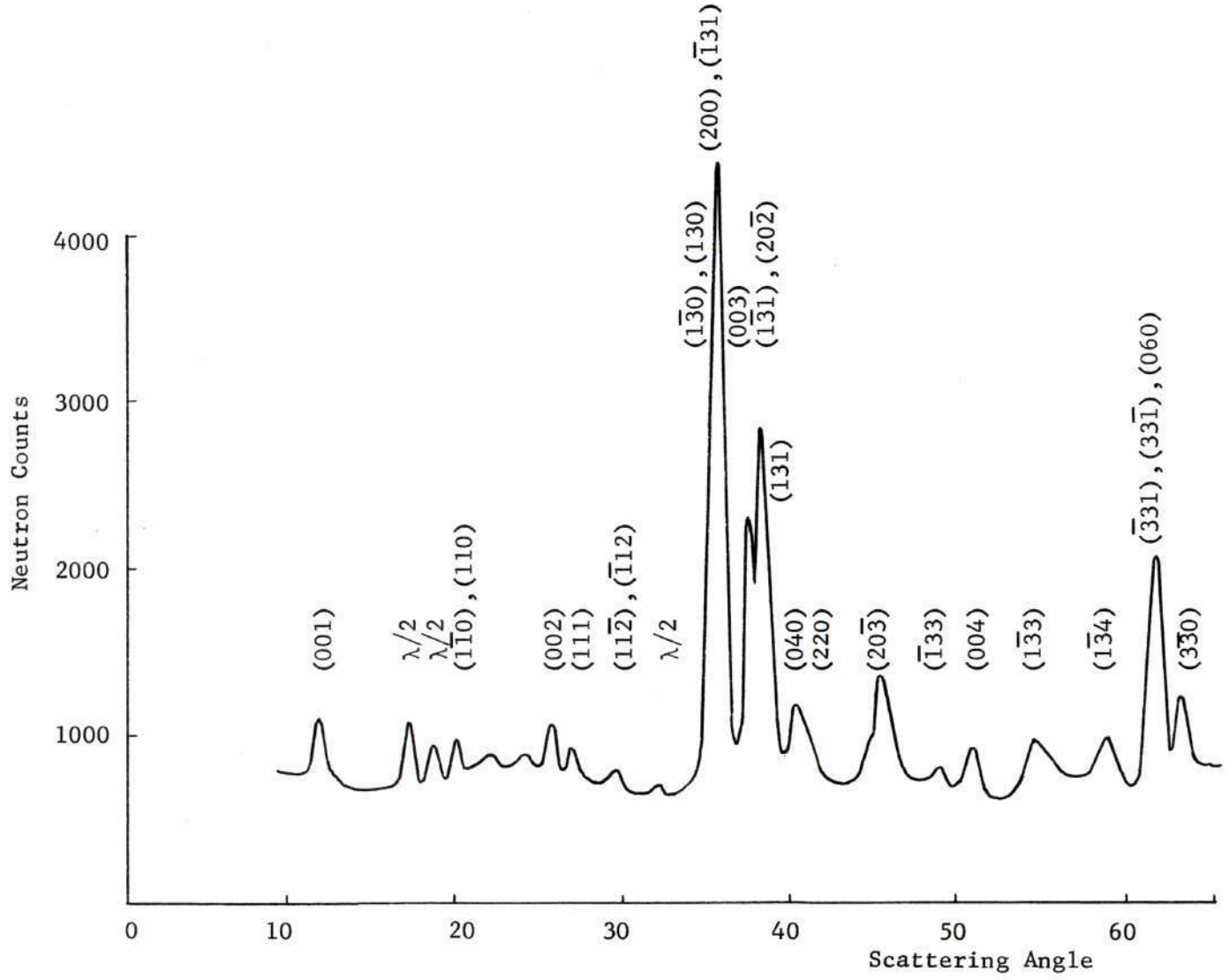

Figure 11. Neutron Diffraction Pattern of Deuterated Kaolinite

of the neutron diffraction pattern was the existence of a large diffuse background. This was attributed to the remaining 7 percent hydrogen content of the deuterated kaolinite sample, multiple scattering, and air scattering. Air scattering also contributed to an increasing peak base line with decreasing scattering angle.

Structure Analysis of Deuterated Kaolinite

The method of attacking the deuterated kaolinite structure problem consisted of three phases of computer pattern generation to achieve a best fit of experimental data. The analysis began with an examination of proposed kaolinite models and the effect of deuterium substitutions. After the selection of the best general model, variations were made in deuterium coordinates to achieve a better fit. Final structural analysis was made by moving structural units within the unit cell and slight variations of deuterium coordinates.

Proposed Kaolinite Models. Computer patterns were generated for models proposed by Brindley and Robinson, Sanders, and Drits and Kashaev. These models represent accepted kaolinite structures and vary in the degree of structural distortion. To consider deuterium in the models proposed by Brindley and Robinson and Drits and Kashaev coordinates equivalent to Sanders' proposed hydrogen positions were assumed. None of the models offered a good fit to the experimental pattern indicating that a large amount of structural refinement would be required (see Figures 12-14). The Sanders' model was selected as the basis for further structural analysis because relative peak intensities from 35°-45° 2θ offered the best agreement with the corresponding most predominant exper-

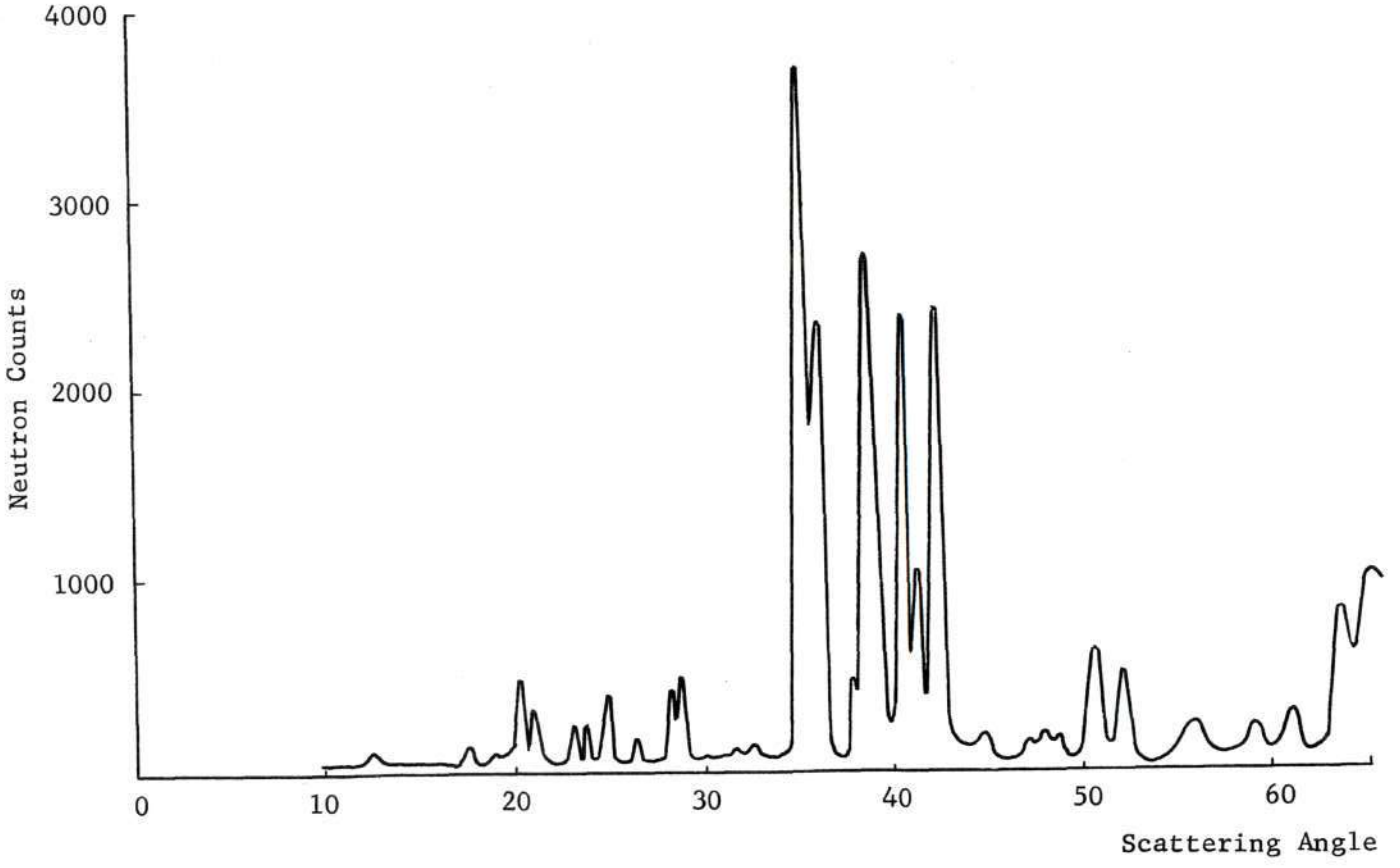

Figure 12. Deuterated Kaolinite with Coordinates Proposed by Brindley and Robinson

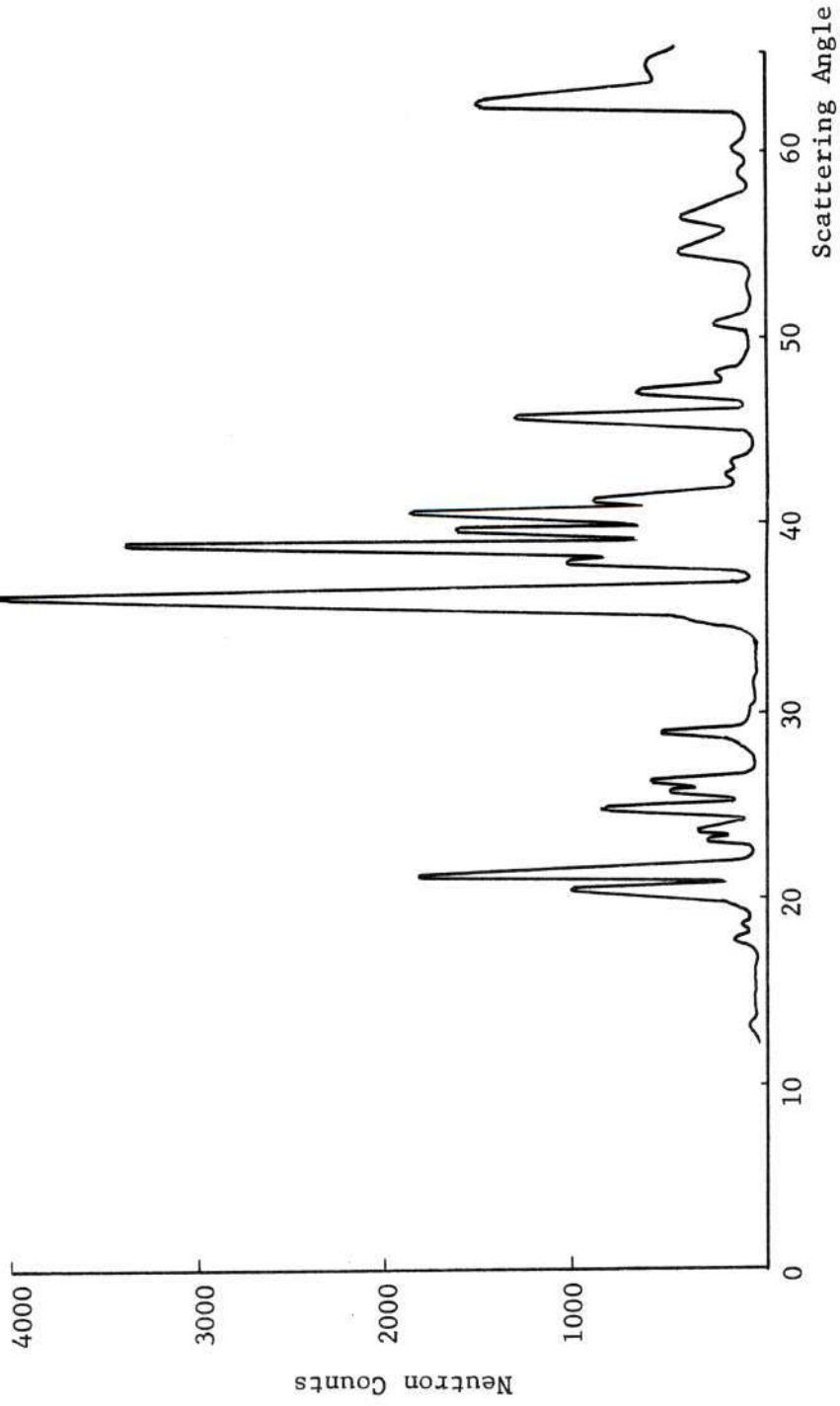

Figure 13. Deuterated Kaolinite with Coordinates Proposed by Sanders

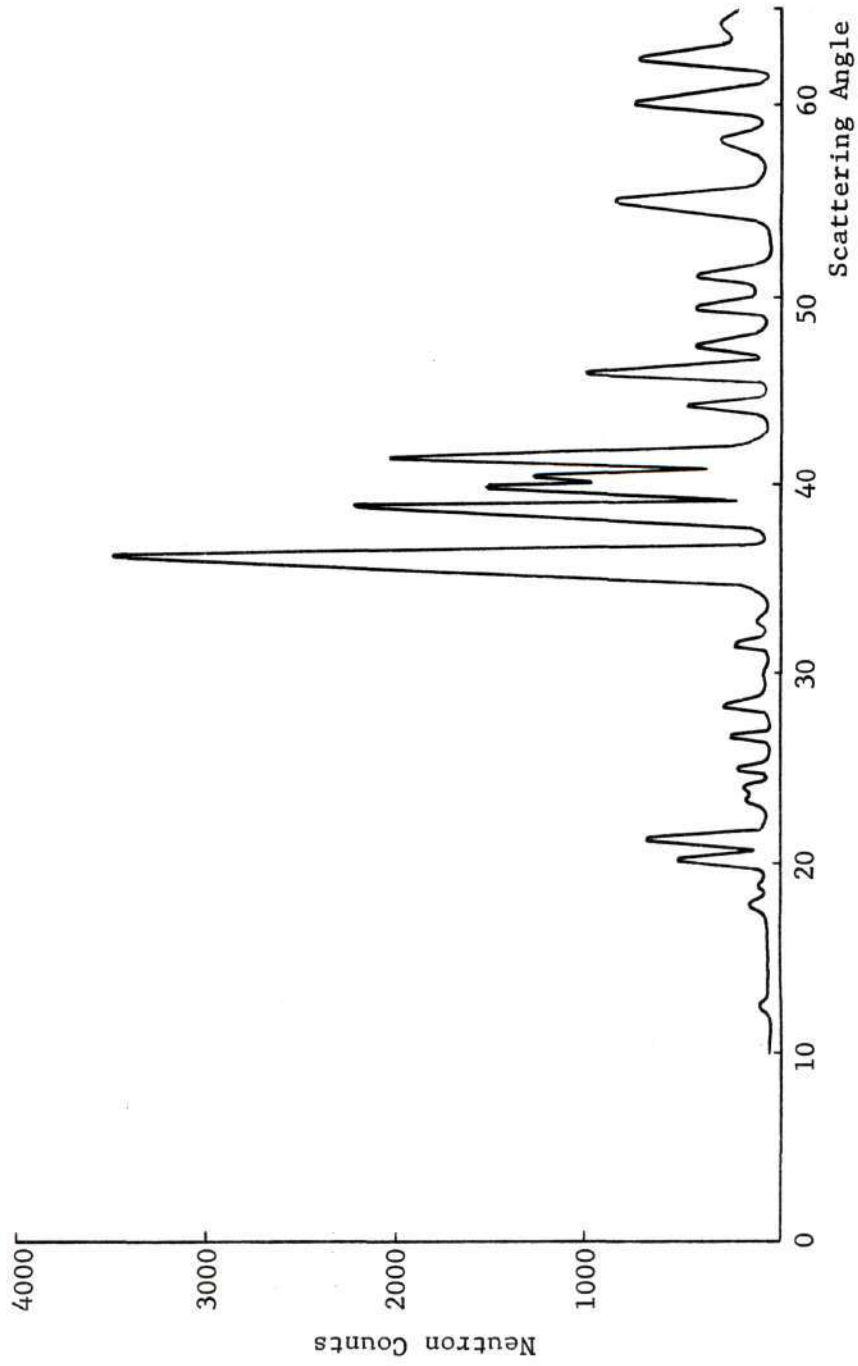

Figure 14. Deuterated Kaolinite with Coordinates Proposed by Drits and Kashaev

imental peaks. For a rough structure analysis, the non-deuterium atomic coordinates proposed by Sanders were assumed to be correct and variations made on deuterium positions.

Variation of Deuterium Coordinates. An initial investigation was performed to calculate the effects of hemispherically varying deuterium positions. Sanders' proposed model placed hydrogen atoms H_1, H_2, and H_3 above the oxygen plane of z = .593 at z = .723 and H_4 below the oxygen plane of z = .300 at z = .165 (see Figure 1). Models were generated placing D_1, D_2, and D_3 below the oxygen plane at z = .465 and D_4 above its corresponding oxygen plane at z = .465. Various combinations redirecting individual atoms while others were held constant in their proposed coordinates were also tried. Hemispherical variations did not produce any positive results, as expected. It was logical that D_1, D_2, D_3, and D_4 be located away from the octahedral sheet with its highly charged aluminum cations. Another possibility that still remained was that D_4 could occupy a random position as suggested by early infrared spectroscopic investigations of kaolinite. The possibility of this was eliminated by assigning D_4 the coordinates of its associated oxygen and observing a resultant increase in pattern disagreement. The conclusion that D_1, D_2, and D_3 were directed upward and D_4 downward was confirmed.

Exact variations of deuterium coordinates from those proposed by Sanders were made by assuming an OD bond length and varying the orientation of OD bonds with respect to the c-axis. Variation of OD_1, OD_2, and OD_3 were made with D_4 fixed in the proposed position. Four variations of bond orientation were made making OD_1, OD_2, and OD_3 perpendicular to the

ab-plane, parallel to the c-axis, and placed in two intermediate orientations. These changes affected the diffraction pattern predominantly in the 35° - 40° 2θ angular range and indicated that bond orientations of an intermediate type provide the best fit (see Figure 15). At this point in the structure analysis, the most acceptable deuterium coordinates appeared to be those in Table 8.

Table 8. Suggested Deuterium Coordinates

Atom	x	y	z
D_1	.667	.000	.759
D_2	.167	.167	.759
D_3	.667	.333	.759
D_4	.543	.481	.165

Thus, upper OD bonds are not perpendicular to the ab-plane as suggested by several infrared investigations. To eliminate other possible bond orientations, OD_1, OD_2, and OD_3 were made more perpendicular to the c-axis and also directed toward oxygens in the basal plane of an above unit cell. The effect of both changes enhanced the disagreement with the experimental pattern (see Figure 16). This suggested that OD bond orientations were not directed toward above nearest neighbor oxygens as the proposed OH bonds in Sanders model.

Similar variations were made for OD_4 bonds making them perpendicu-

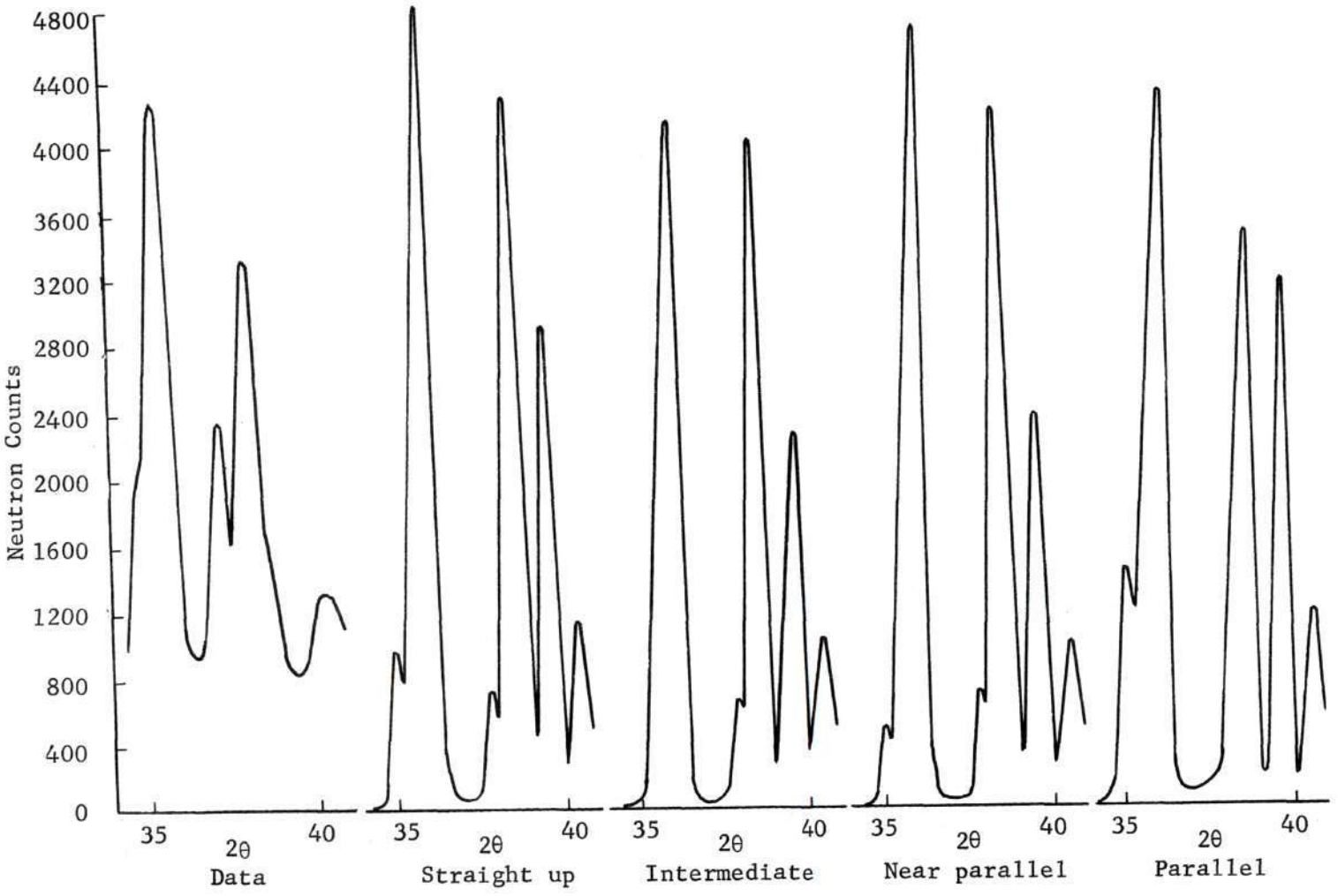

Figure 15. Neutron Diffraction Pattern Effects Caused by Changing OD_1, OD_2, and OD_3 Bond Orientations Relative to the c-Axis

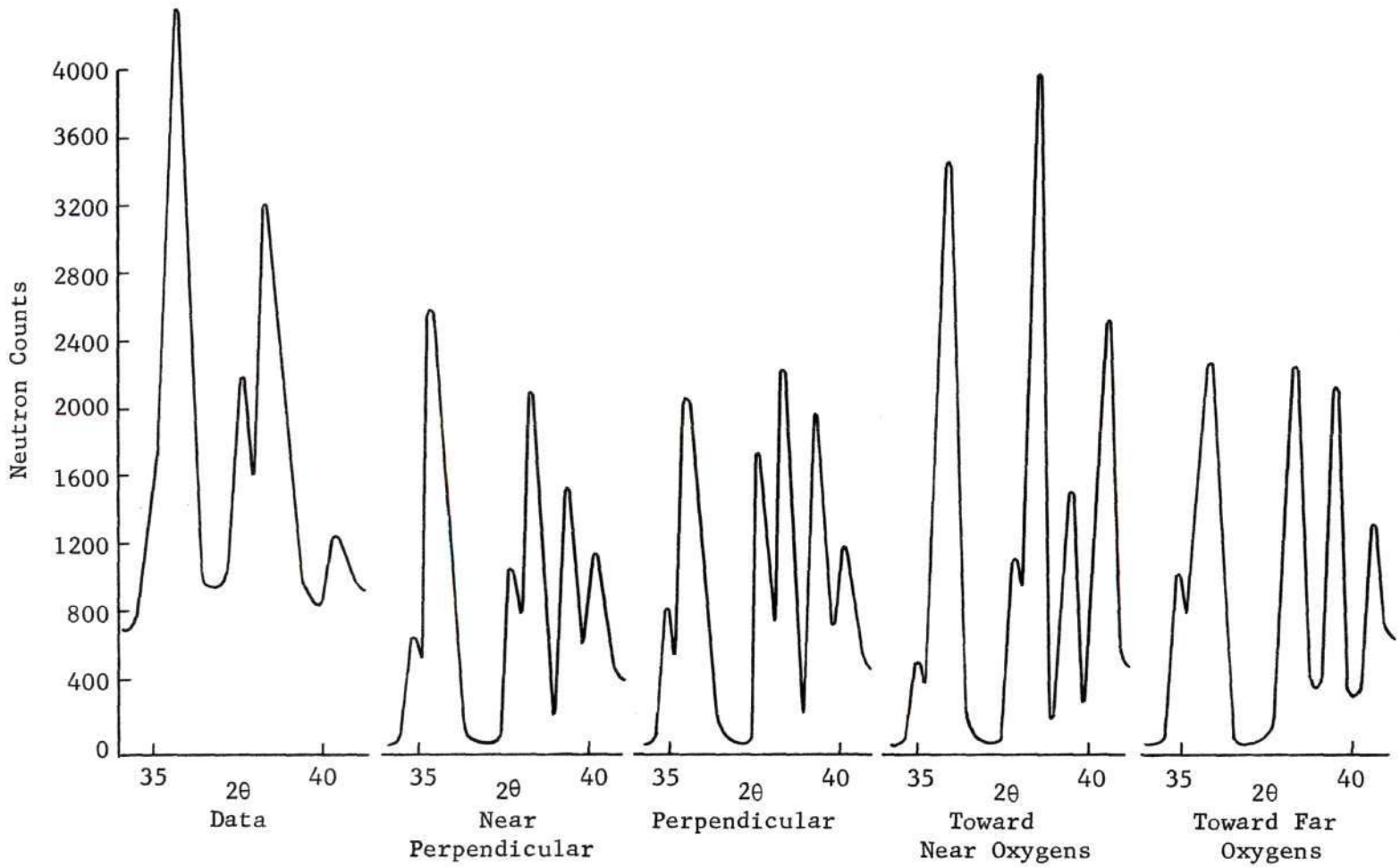

Figure 16. Neutron Diffraction Pattern Effects Caused by Varying OD_1, OD_2, and OD_3 Bond Orientations

lar to the ab-plane, more perpendicular to the c-axis, and also redirecting them toward near oxygens in the tetrahedron bases. Variations in OD_4 orientations predominantly affected peaks in the 20° - 25° 2θ range with no improvements made for any of the changes (see Figures 17 and 18). Consequently, the proposed D_4 coordinate was not changed and the calculated pattern still did not represent a good fit.

The examination of the new coordinates relative to those proposed by Sanders indicated only small variations existed in certain plane projections while large differences existed in others. Attempts to improve the fit were made by coinciding deuteriums with proposed hydrogen coordinates in various plane projections. In the (001) projection coinciding D_1 with H_1 and D_2 with H_2 failed to improve agreement even though only minor differences existed between the coordinate sets (see Figure 19). The largest discrepancy was visible in the (001) projection with D_3 and H_3 being nearly 180° away from each other on opposite sides of the hydroxyl oxygen. Attempts to move D_3 into closer agreement with H_3 increased pattern disagreement. Similar experiments were tried for the (100) projection where D_1 and D_4 coincided perfectly with H_1 and H_4 and only small adjustments were required for D_2 and D_3 (see Figure 19). Variations were not successful in improving the fit. The (010) projection was not examined since variations would be duplicated, but it was noted that changes in z for deuteriums might improve the calculated pattern.

Several z values for D_1, D_2, and D_3 were tried ranging from .700 to .789 with the pattern effects illustrated in Figure 20. Best agreement

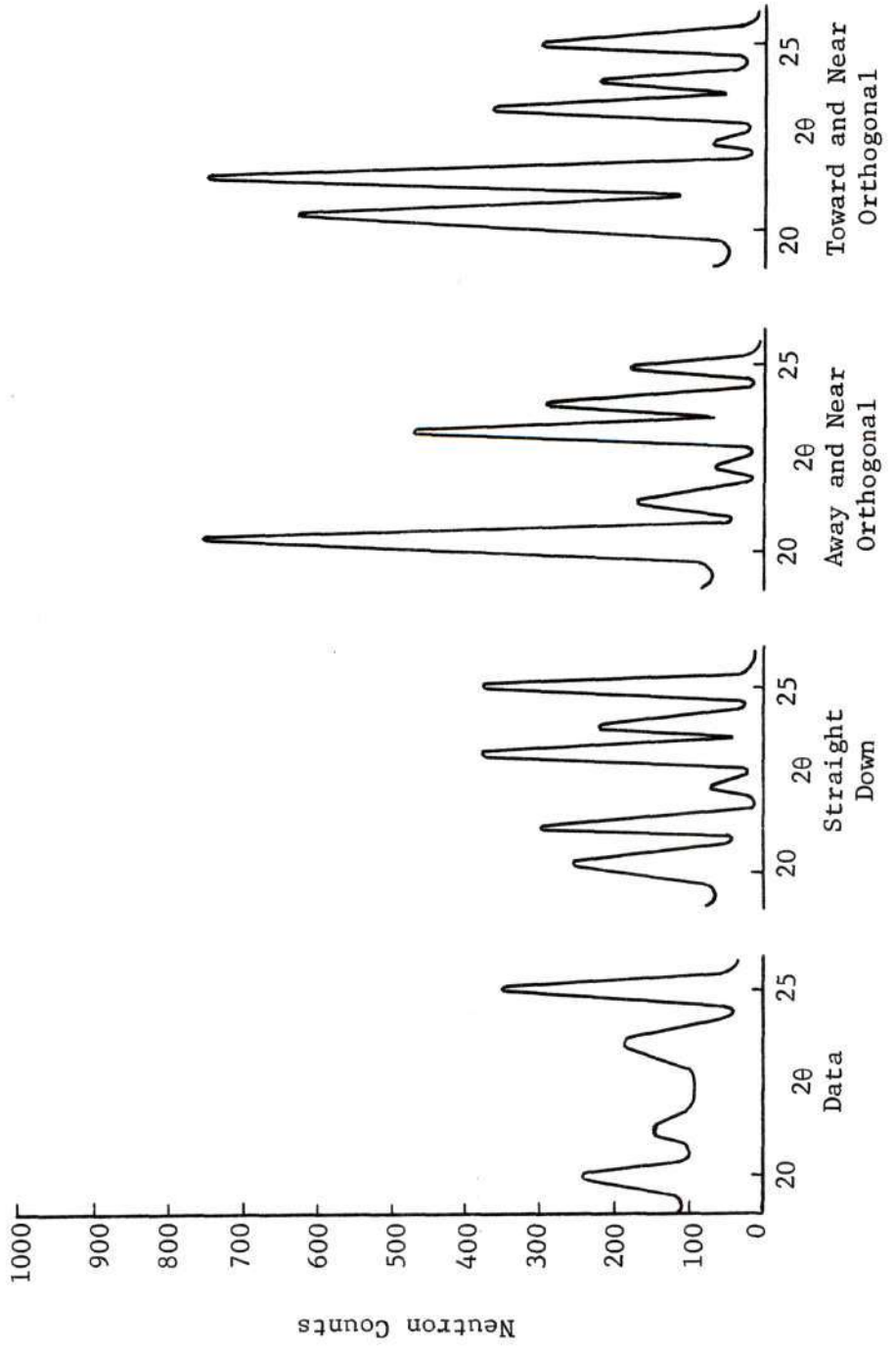

Figure 17. Neutron Diffraction Pattern Effect of Varying OD_4 Bond Orientations

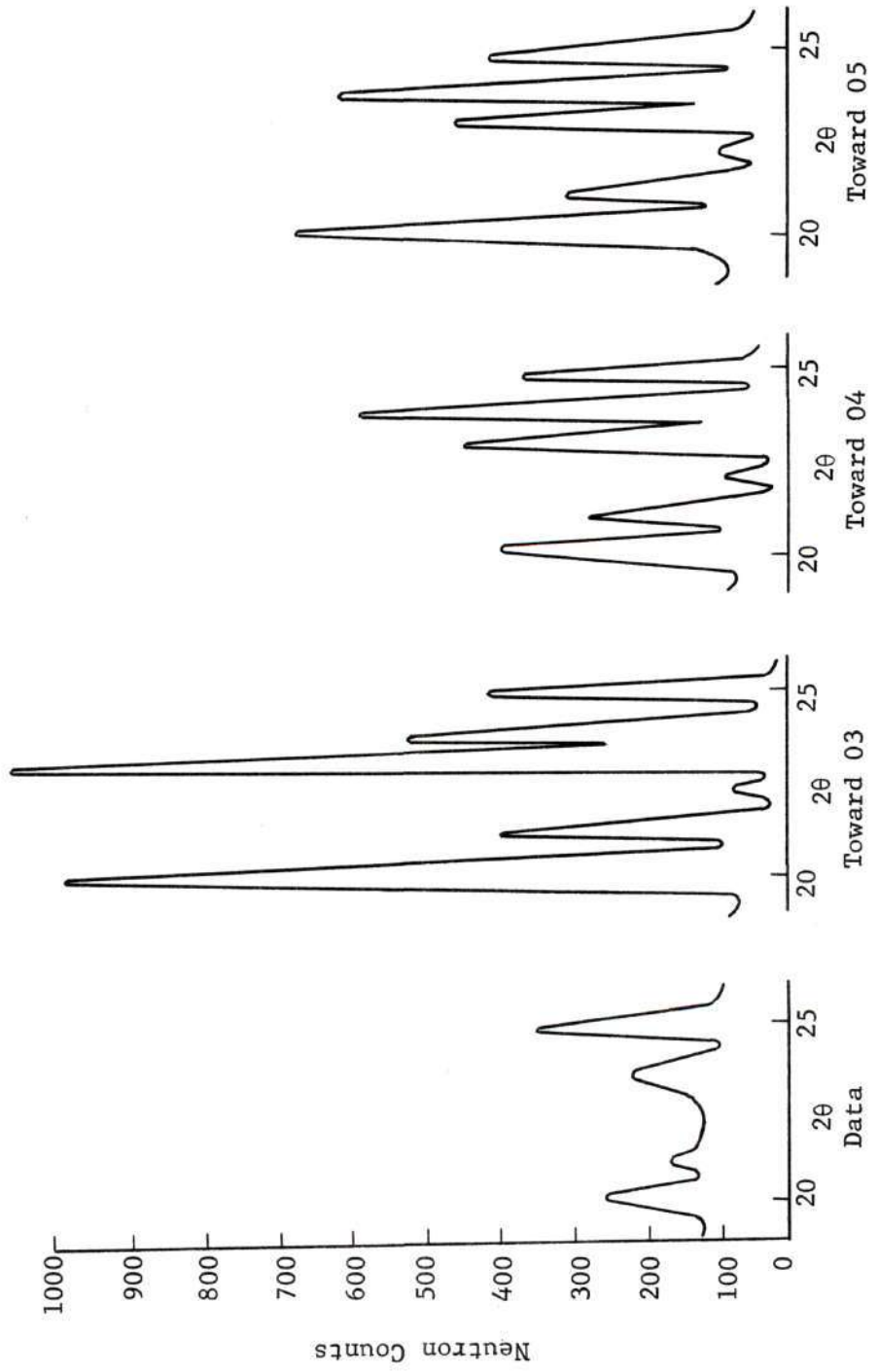

Figure 18. Neutron Diffraction Pattern Effect of Directing OD_4 Bonds Toward Basal Oxygens

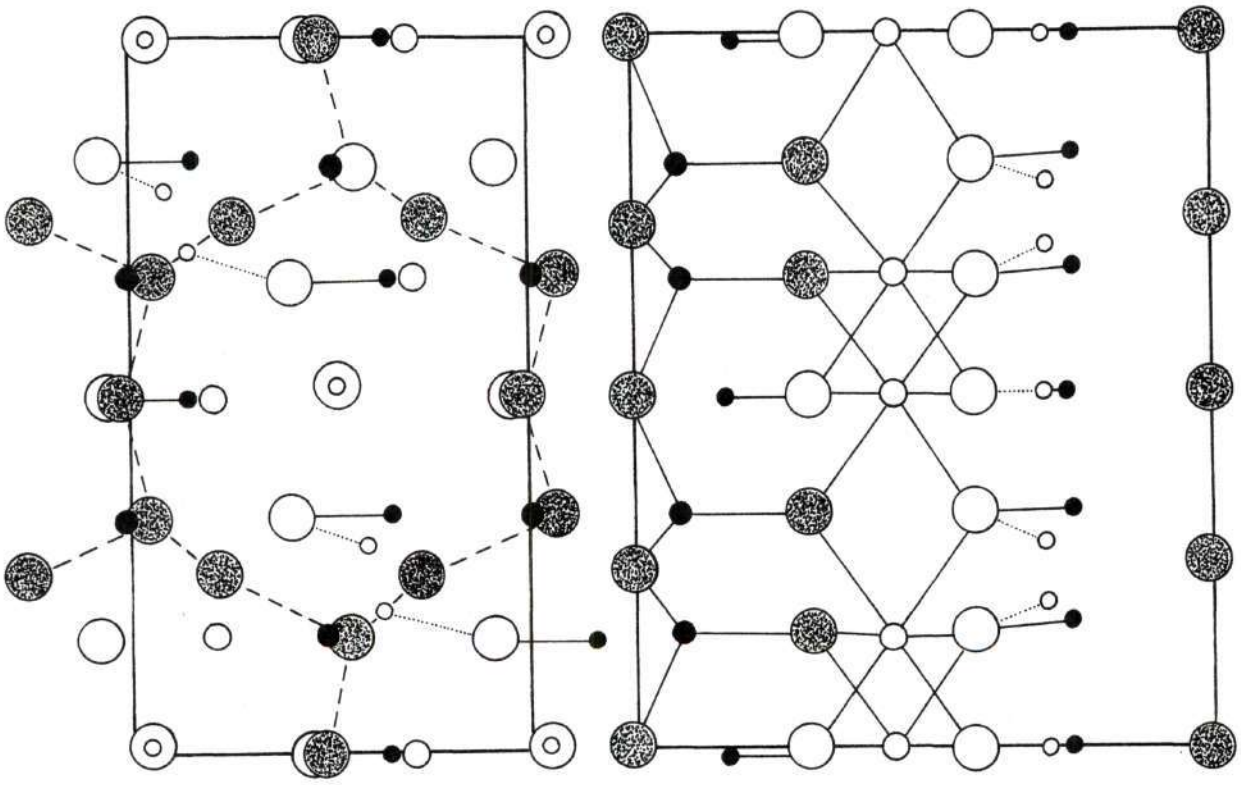

(a) (001) Plane

(b) (100) Plane

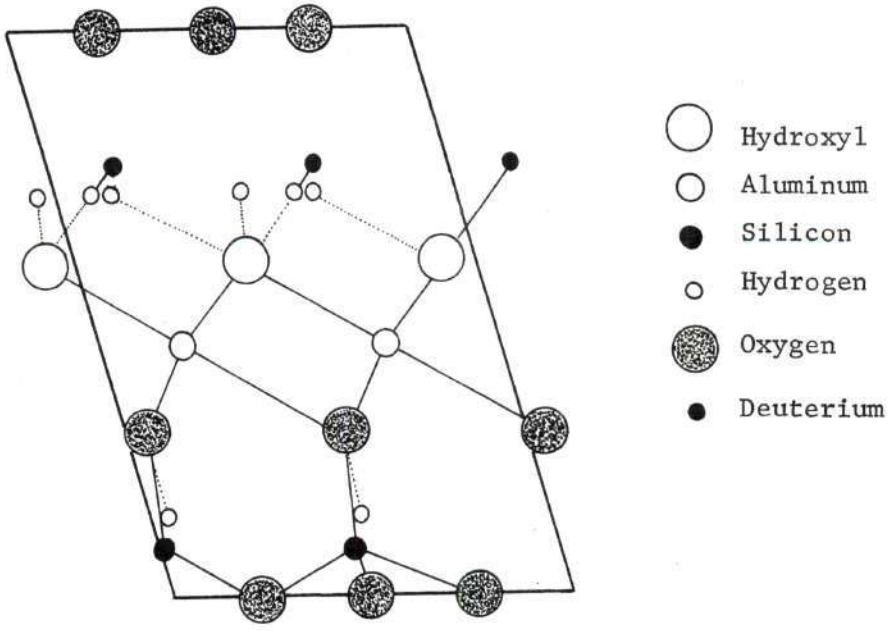

(c) (010) Plane

Figure 19. Comparison of Deuterium and Hydrogen Positions Projected on Various Planes

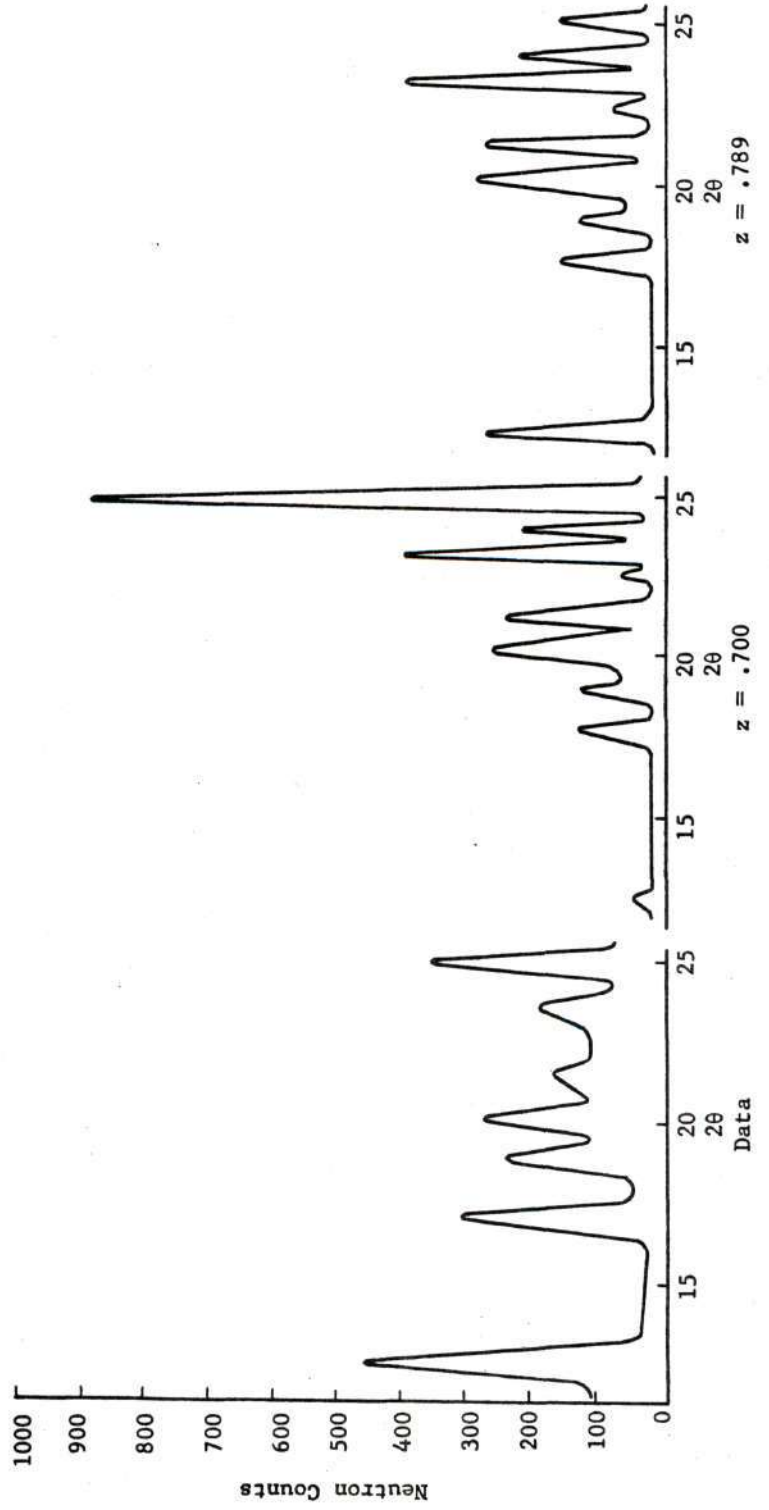

Figure 20. Pattern Effects Resulting from Changing z for D_1, D_2, and D_3

was found adjusting the z-displacement to .770. An investigation was also made for D_4 with a lengthened bond length giving best agreement at z = .150 (see Figure 21). Deuterium coordinates had been adjusted to improve the agreement but good agreement still did not exist with experimental data. The possibility that hydrogen had selectively remained in the kaolinite lattice existed and could have possibly accounted for the remaining pattern discrepancies.

Substitution of hydrogen selectively for individual deuterium atoms improved agreement of 001 type reflections but increased disagreement in the 20° - 25° 2θ range and at higher angles (see Figure 22). From this and the hydrogen content analysis, it was concluded that structural hydrogen did not remain in the deuterated kaolinite.

A reexamination of Sanders' kaolinite model revealed that the deuterium positions so far obtained in the structure did not generate a good fit of the experimental kaolinite pattern. Several adjustments were tried but Sanders' proposed coordinates represented the most refined hydrogen coordinates. This suggested that deuterium coordinates in deuterated kaolinite were not in equivalent positions to hydrogen in kaolinite. It was also evident from the poorness of fit between the calculated deuterated kaolinite pattern and the experimental one that other structural changes had occurred as a consequence of hydrothermal treatment.

The final phase of the structure analysis was to investigate possible structural changes that might occur from hydrothermal reconstitution. To conserve time it was decided that structural units within the unit cell be moved and distorted rather than individual atoms.

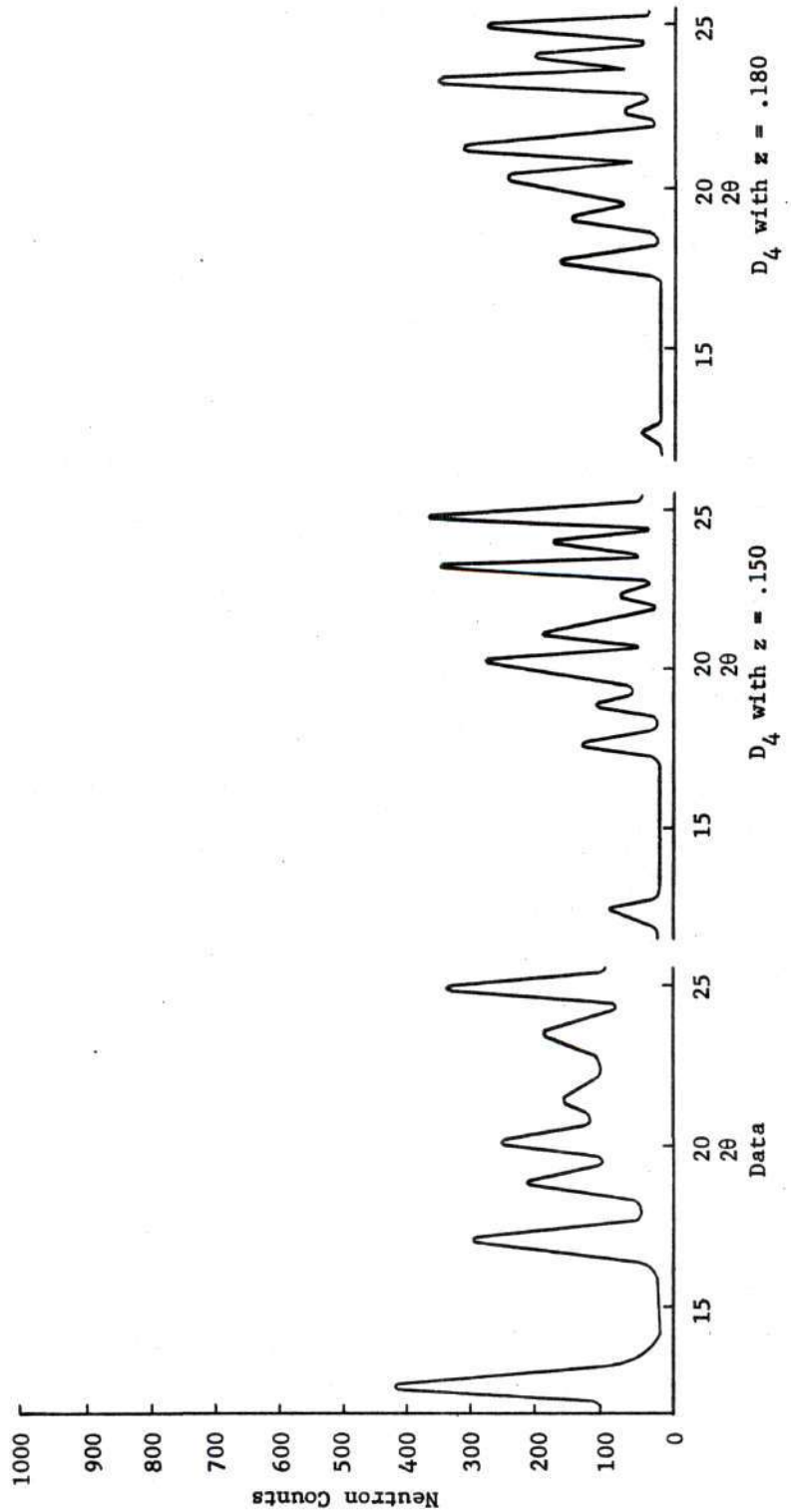

Figure 21. The Effect of Changing z for D_4 on the Calculated Neutron Diffraction Pattern

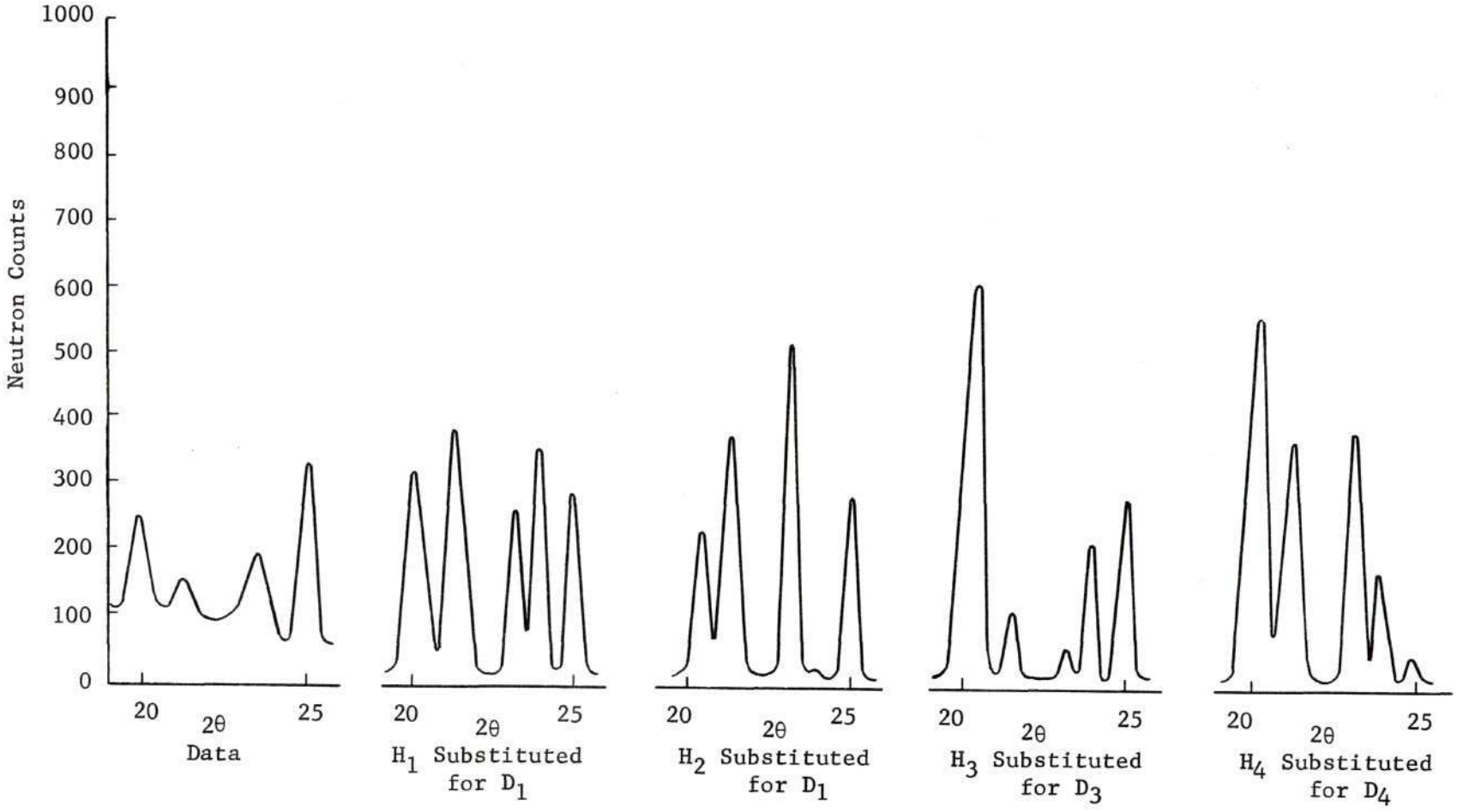

Figure 22. Effects of Selective Hydrogen-Deuterium Substitution on Calculated Patterns

Variations of Non-Deuterium Atomic Coordinates. A rotation of Si-O tetrahedrons was considered to be a possible effect of reconstitution and was investigated by rotation of tetrahedral units 2.5° and 5.0°. Increased rotation resulted in an increase in disagreement between the two major peaks and was eliminated as a possible structural modification (see Figure 23).

Differences in superposition of the octahedral layer on the silica tetrahedral net are characteristic of varying degrees of kaolinite crystallinity. To obtain superposition effects it was only necessary to consider changes in Al positions since hydroxyl oxygens were shifted to equivalent sites. Three possible combinations of Al lattice sites existed depending on whether the deuterated kaolinite could be considered a well crystallized kaolinite, a poorly crystallized fireclay, or as some intermediate crystallinity. Results indicated that both the well crystallized and fireclay coordinates offered suitable patterns (see Figure 24). Until other possible structural changes were considered, the working model coordinates proposed for the well crystallized variety were used.

The above concept of layer superposition suggested that Al cations might be statistically distributed over several of the six possible octahedral sites. It was necessary to define only three lattice sites, since the others were generated by the C Face Centering translation operation in the program. Statistical weights were assigned to possible locations by weighting the Al scattering factors according to the probability of existing in a given site. Patterns indicated that distribution was favored on sites proposed for a well crystallized kaolinite (see Figure 25).

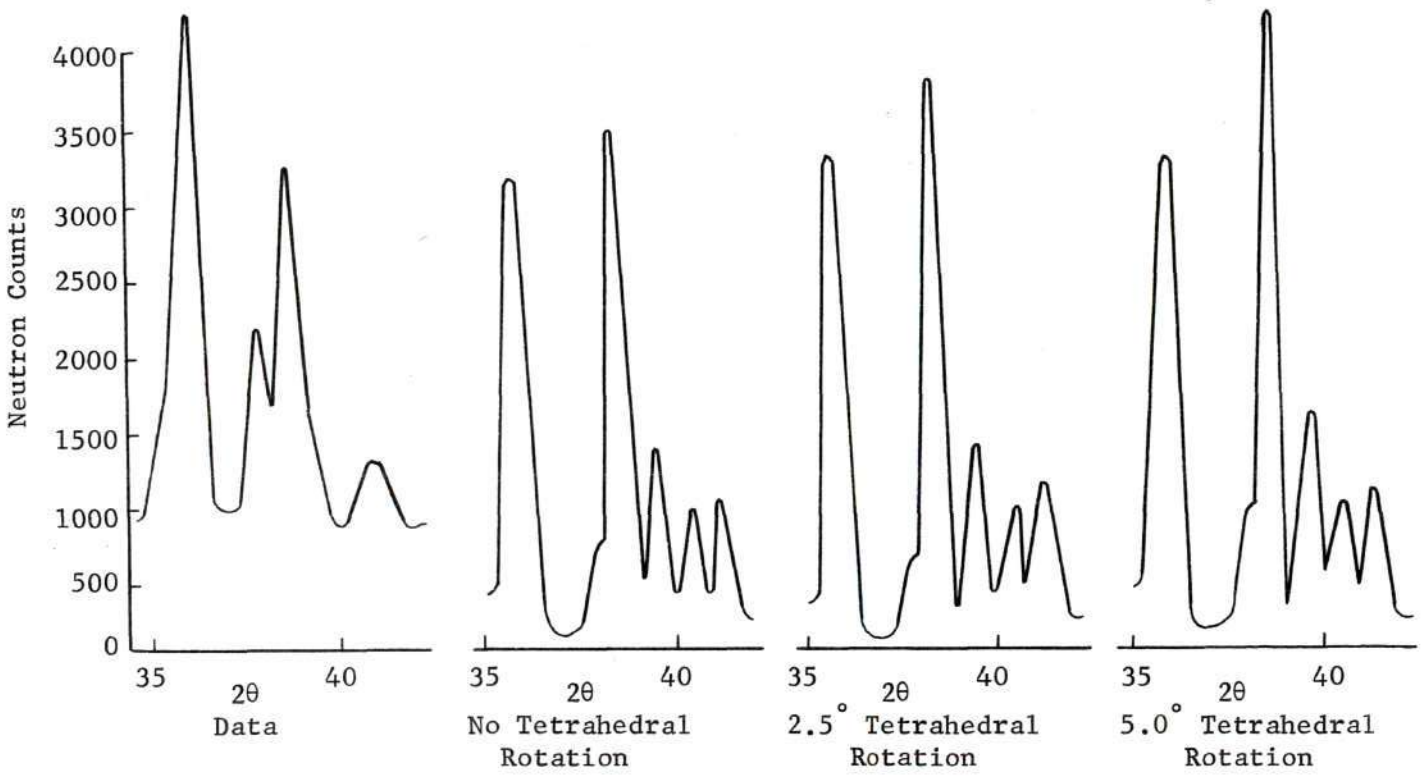

Figure 23. The Effect of Tetrahedral Rotation on a Deuterated Kaolinite Neutron Diffraction Pattern

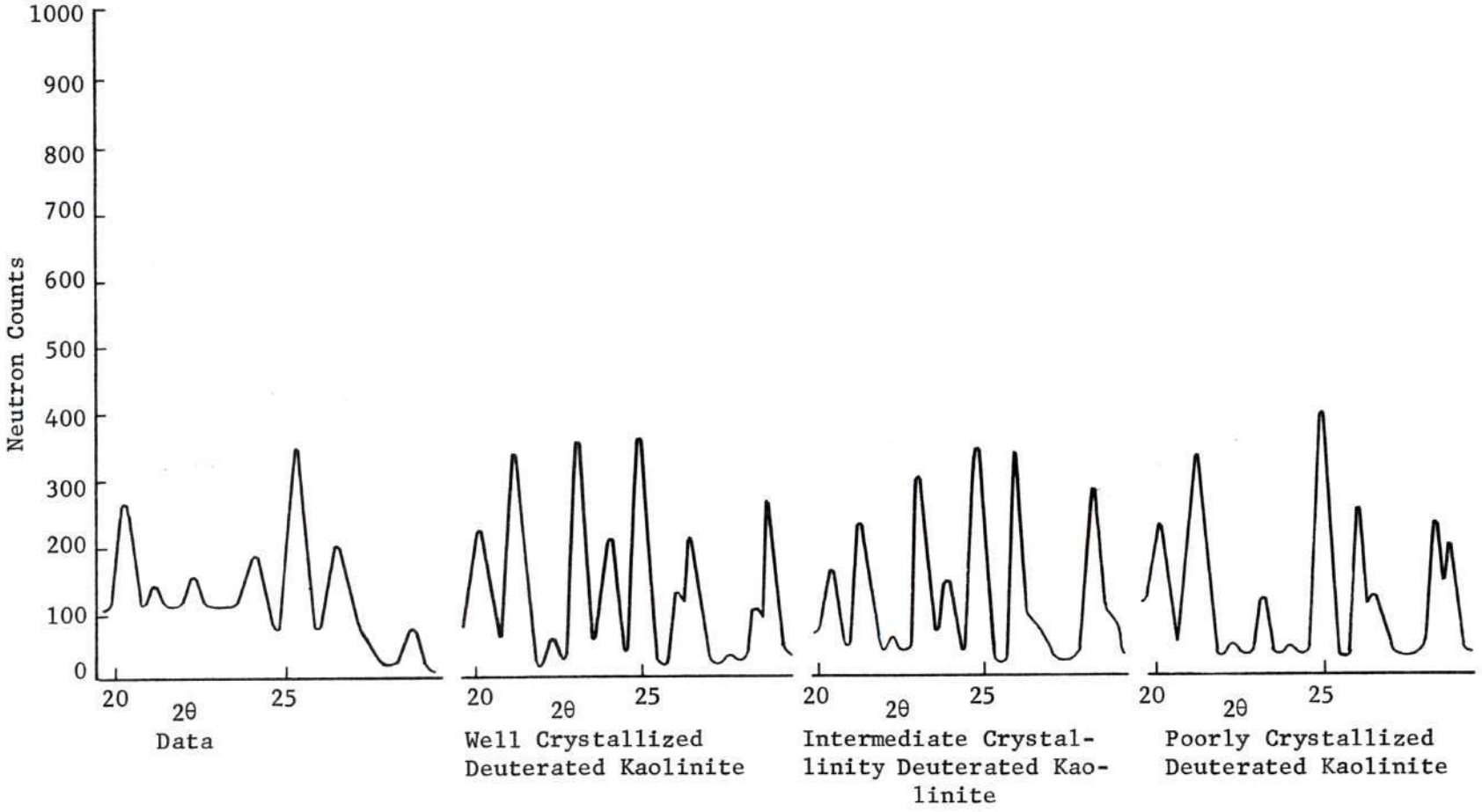

Figure 24. Pattern Changes Due to Varying Al-O, OH Layer Superposition

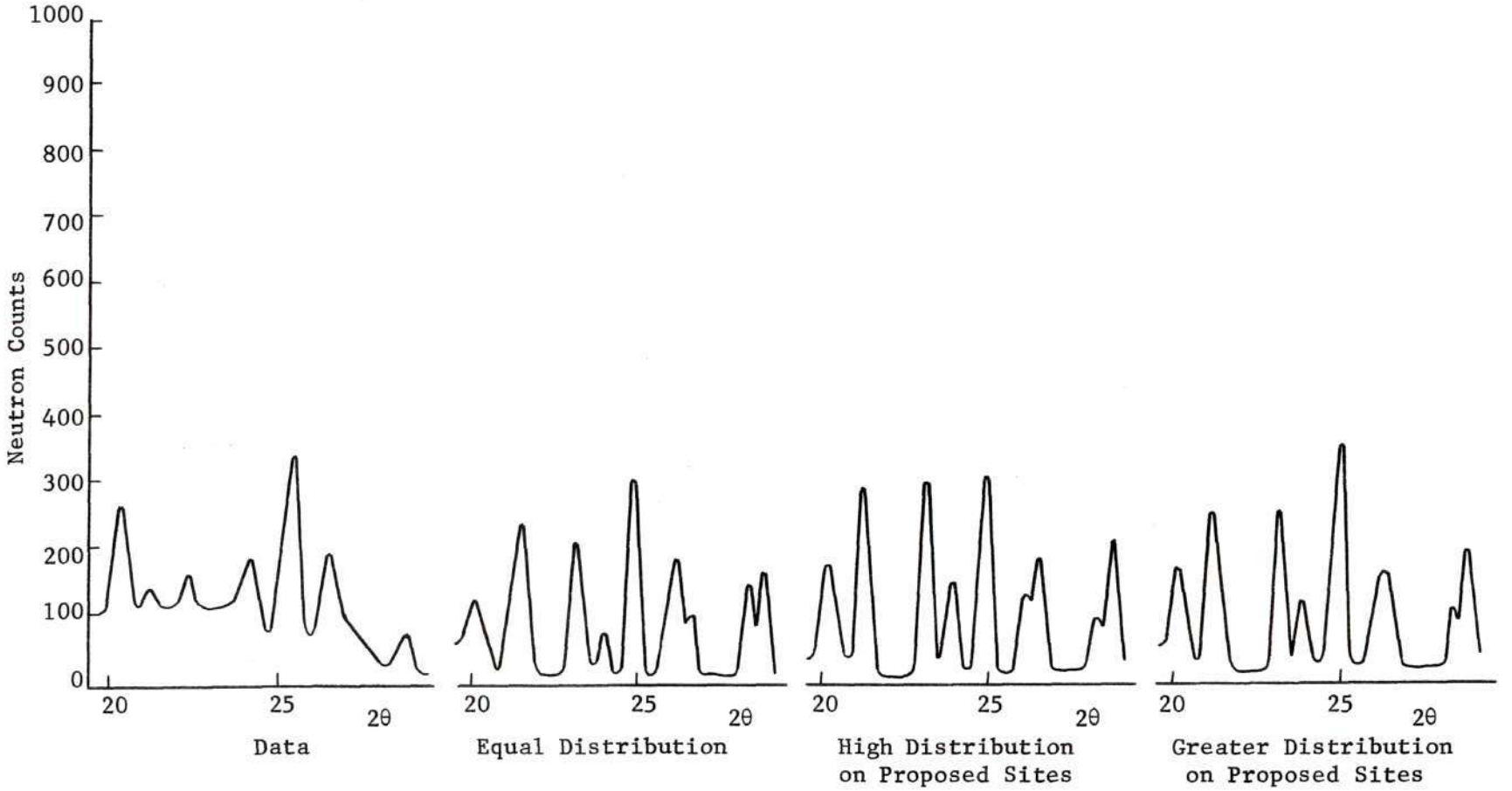

Figure 25. Pattern Effects Due to Statistical Distribution of Al Cations on Available Sites

Another structural variation characteristic of kaolinite group minerals is the possibility of nb/3 layer shifts analogous to stacking fault effects in metals. Consideration of the reciprocal space lattice construction for a layered silicate like kaolinite revealed that the effect of a shift of one-third the b-axis would draw out reciprocal lattice points of reflections with k/3 fractional parallel to the c* axis. The effect on the neutron diffraction pattern would be to broaden these reflections and cause an apparent decrease in intensity. At the same time reflections with k/3 integral would remain sharp and unaffected. Great improvement was made in fitting the model to the experimental pattern when this adjustment was incorporated into the program calculations. A fairly high probability of a nb/3 shift was required to obtain the best results (see Figure 26). With significant pattern improvements, slight variations of deuterium coordinates were again tried and a better fit found using the following coordinates listed in Table 9.

Table 9. Final Deuterium Coordinates

Atom	x	y	z
D_1	.595	.000	.770
D_2	.095	.167	.770
D_3	.595	.333	.770
D_4	.543	.481	.150

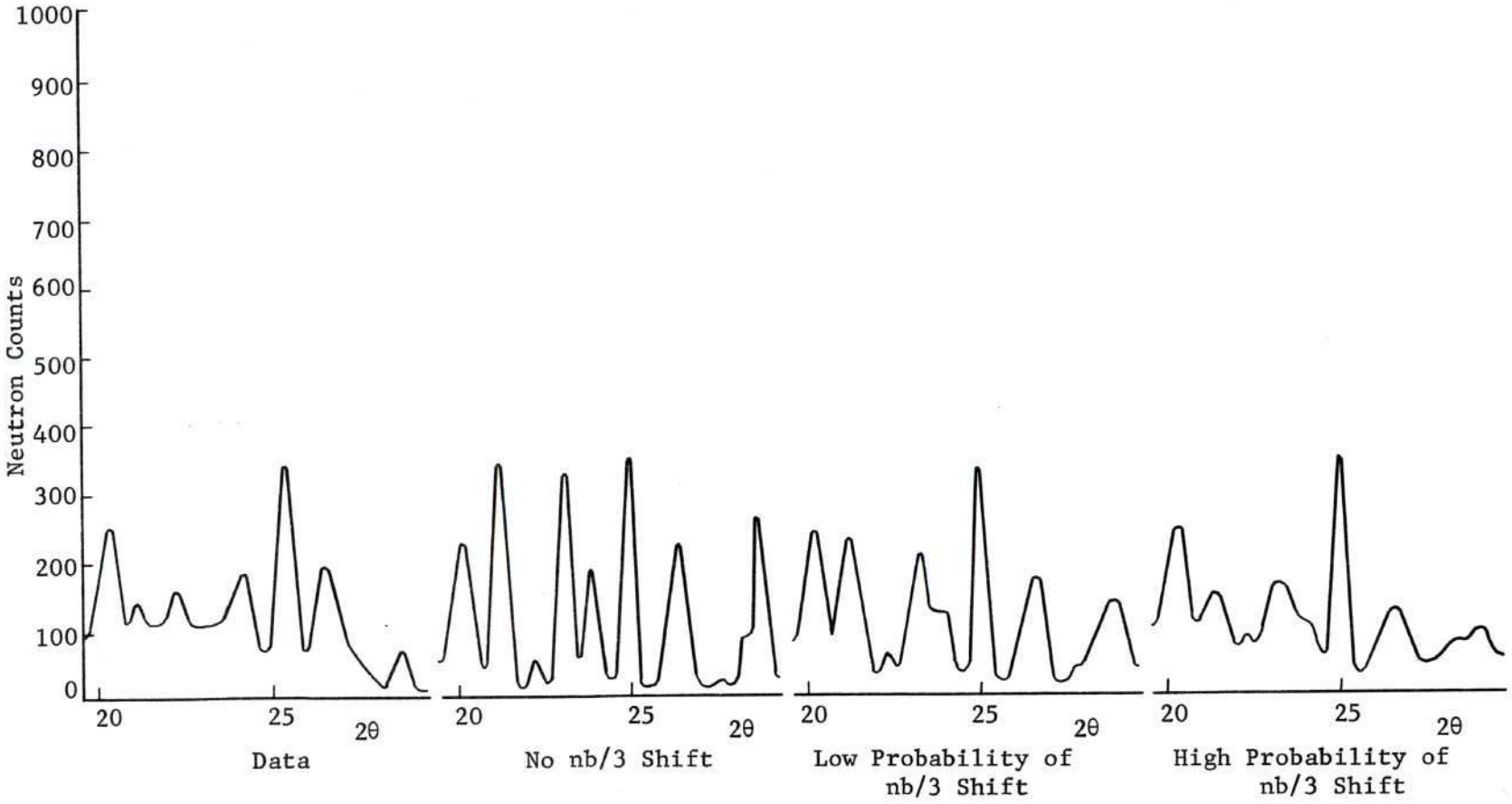

Figure 26. The Effect of nb/3 Shifting on Calculated Diffraction Patterns of Deuterated Kaolinite

The improved coordinates contain slight changes in x and z for D_1, D_2, and D_3, and in z for D_4, producing a good fit (see Figure 27).

An additional structural modification was made in an attempt to obtain better agreement between 001 type reflections by puckering the basal plane. The result of the displacements of basal oxygens increased reflection intensities but did not improve the relative fit to the experimental pattern. It was concluded that puckering of the basal plane did not occur as a result of hydrothermal reconstitution (see Figure 28).

Figure 27 can be compared to Figure 11 to discuss the agreement of the calculated fit. In general, there is good correspondence between the calculated pattern and the experimental one when the difference in background is neglected. Some slight discrepancies exist in relative peak intensities. For example, a comparison of the relative intensities of the two major peaks indicated that, in the calculated pattern, the second peak, $(1\bar{3}1)$, $(20\bar{2})$, should be less intense. Other minor intensity disagreements existed with the only major problem being the misfit of the (003) reflection intensities. This suggested some error in z displacement within the unit cell other than a basal plane puckering. A comparison of $\lambda/2$ contributions indicated good agreement between the patterns. Peak broadening was found to be slightly different for each case. Calculated broadening contributions included instrumental effects, crystallite size effects, and the degree of nb/3 shifting. Minor differences probably could have been compensated for by the selection of larger instrumental broadening and the inclusion of two-dimensional effects. Incorporating a two-dimensional correction would have improved the agreement in several angular ranges. In particular, in the 2θ range of 40° - 42°,

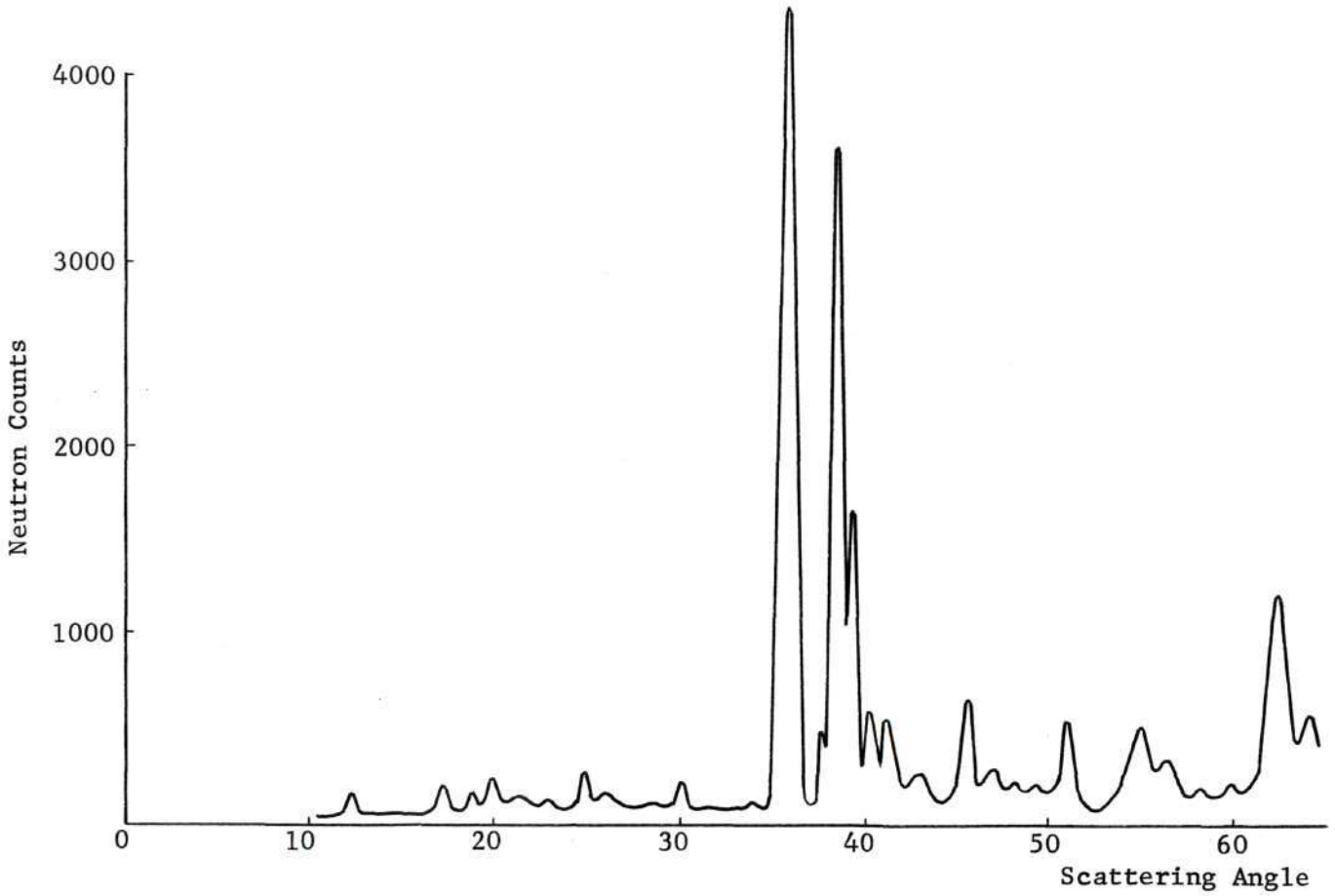

Figure 27. Calculated Pattern for Deuterated Kaolinite with nb/3 Shifting and Best Fit Coordinates

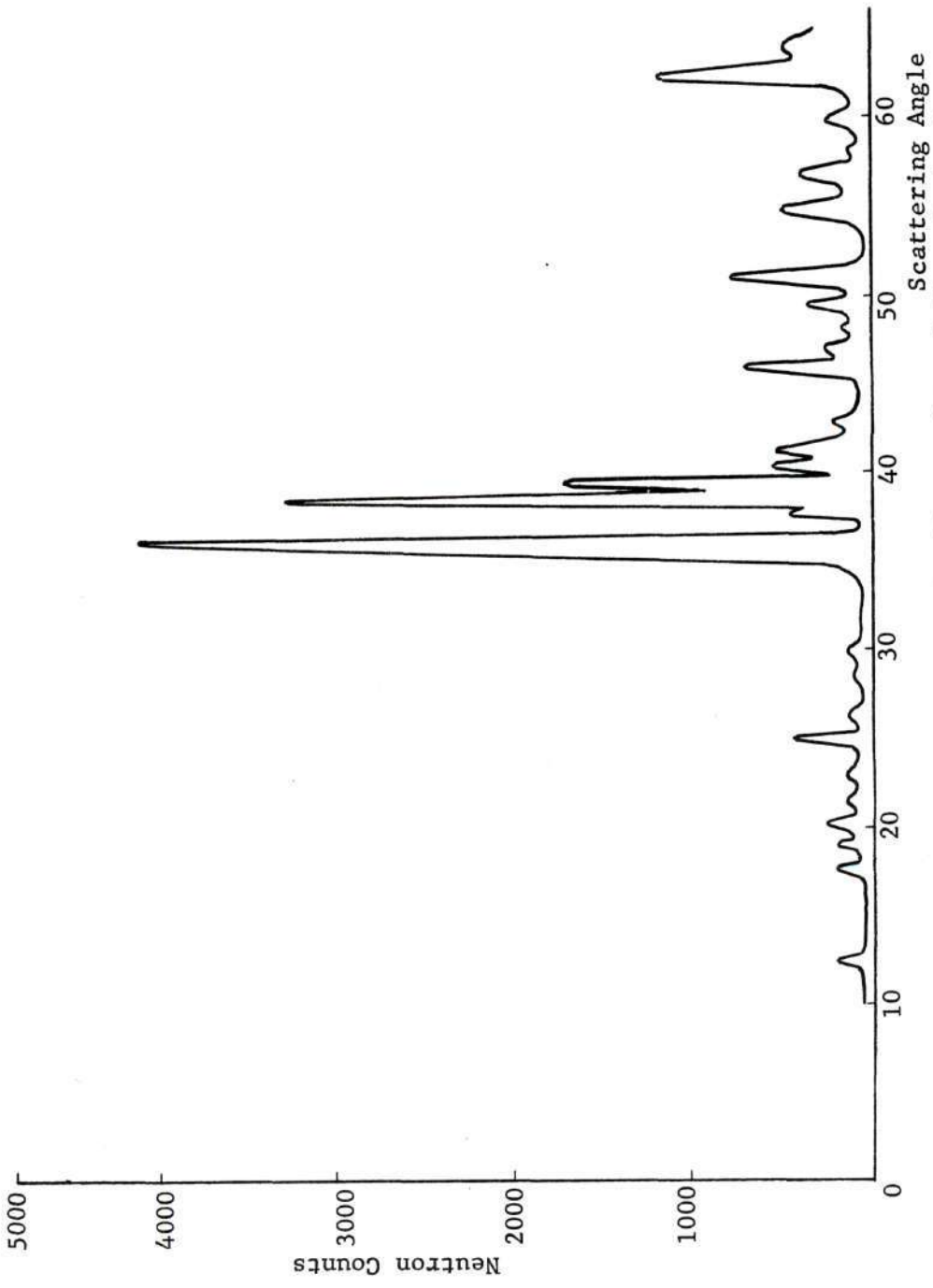

Figure 28. Deuterated Kaolinite with Effects of Basal Plane Puckering on Calculated Pattern

the (220) would have been broadened into the (040) to give one broad peak in the calculated pattern. Other broadening effects especially the nb/3 compensation seem to produce excellent agreement.

The correspondence between the calculated and experimental powder patterns permits the discussion of the reconstituted structure of deuterated kaolinite (see Figure 29). The structure changes due to reconstitution in non-deuterium atoms was small. No major structural modifications within the unit cell could be detected including tetrahedral rotation, octahedral superposition, and basal plane puckering. However, the remaining inconsistencies between the calculated and experimental patterns suggested that errors in individual atomic coordinates probably existed. The most significant effect of reconstitution was the development of high probabilities of nb/3 shifting between unit cells. This can be explained as a direct consequence of the dehydration step resulting in total disorder of the original kaolinite structure and the inability of hydrothermal treatment to be a completely reversible process.

The atomic position of D_3 was found to be significantly different from that proposed by Sanders. However, the finding does not refute the Sanders' model for well crystallized kaolinite. Instead, it is suggested that deuterium does not occupy the same positions as hydrogen in kaolinite. Infrared literature suggested this idea as well as the possibility of increased OD bond length. Considering these effects proposed by infrared spectroscopy, predictable changes in the proposed hydrogen coordinates were shown to occur as a result of hydrothermal deuteration. Results did, however, refute the IR spectroscopic finding that OD bonds were more in-

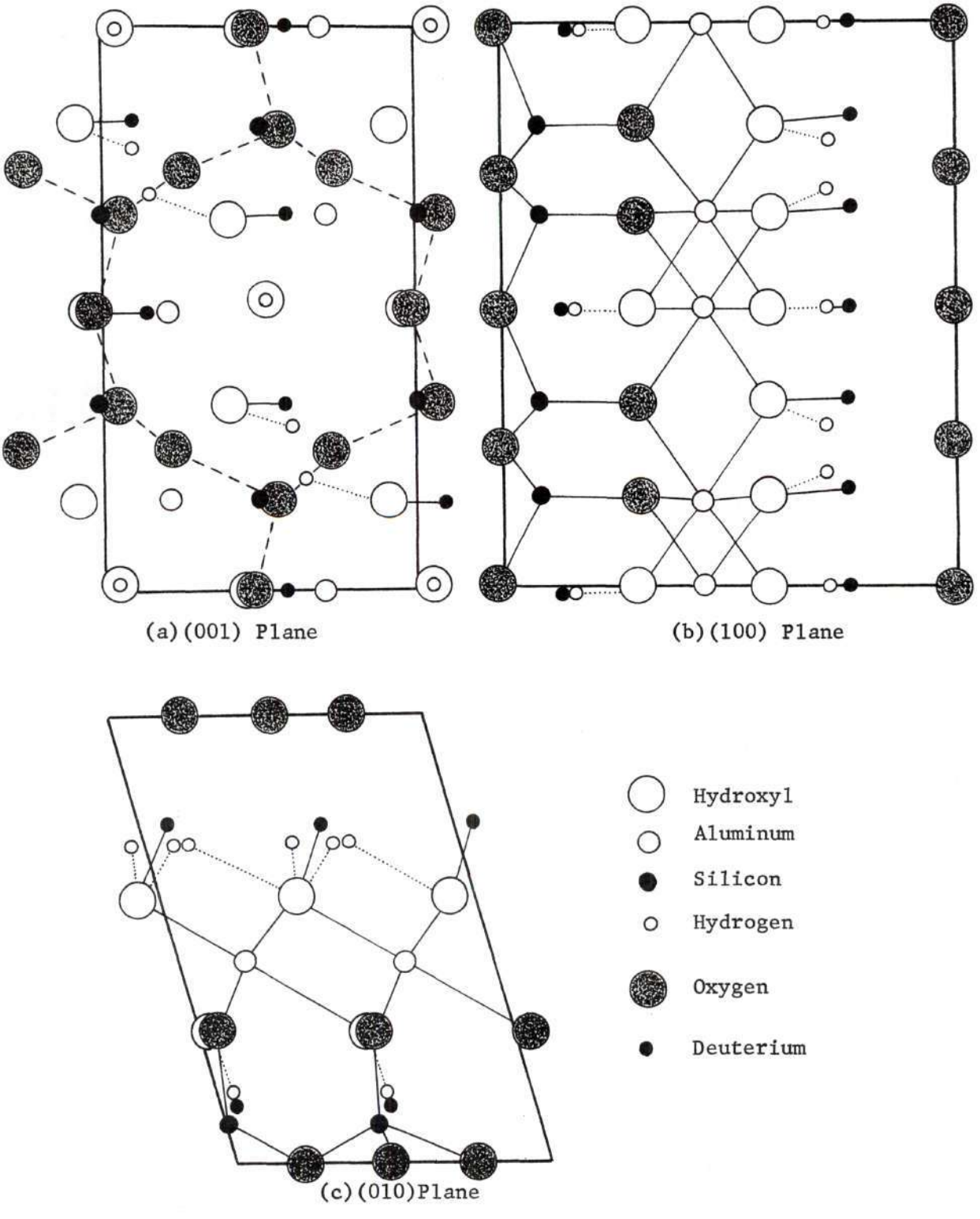

Figure 29. Proposed Deuterium Positions in Deuterated Kaolinite Projected on Various Planes

clined to the ab-plane than initial OH bonds. Figure 29 revealed that only minor coordinate differences existed between D_1, D_2, and D_4, and H_1, H_2, and H_4, respectively. These minor differences might be attributed to a weakening of hydrogen bonds due to the deuterium substitutions. The major discrepancy that was found in the values of the x coordinate for D_3 and H_3 was not readily explainable. One can suggest that it could have occurred as a result of some other disruption within the unit cell developing from the hydrothermal treatment. D_3 appeared to be moved to a position of lowest electrostatic repulsion with respect to the aluminum ion. The new deuterium coordinates were substituted for hydrogens in kaolinite and a neutron diffraction pattern was calculated to check this idea. The resulting kaolinite pattern did not fit the experimental data obtained by Sanders (5). Thus, indicating that the coordinates for hydrogens in kaolinite and deuteriums in deuterated kaolinite were not identical (see Figure 30). This finding eliminated the possibility for refinement of hydrogen coordinates using deuterium substitutions. Rather, valuable information on changes of bond orientations and deuterium locations resulting from hydrothermal treatment has been found.

It should be noted that the proposed deuterium coordinates and OD bond orientations cannot be regarded as refined structural details. Several inconsistencies remained between the calculated and experimental neutron diffraction patterns suggesting that non-deuterium atoms require refinement. Non-deuterium atoms were not moved as might otherwise be done in a true structure refinement. Obviously, not all of the possible deuterium coordinates have been tried and, consequently, the proposed positions represent the most suitable relative deuterium coordinates.

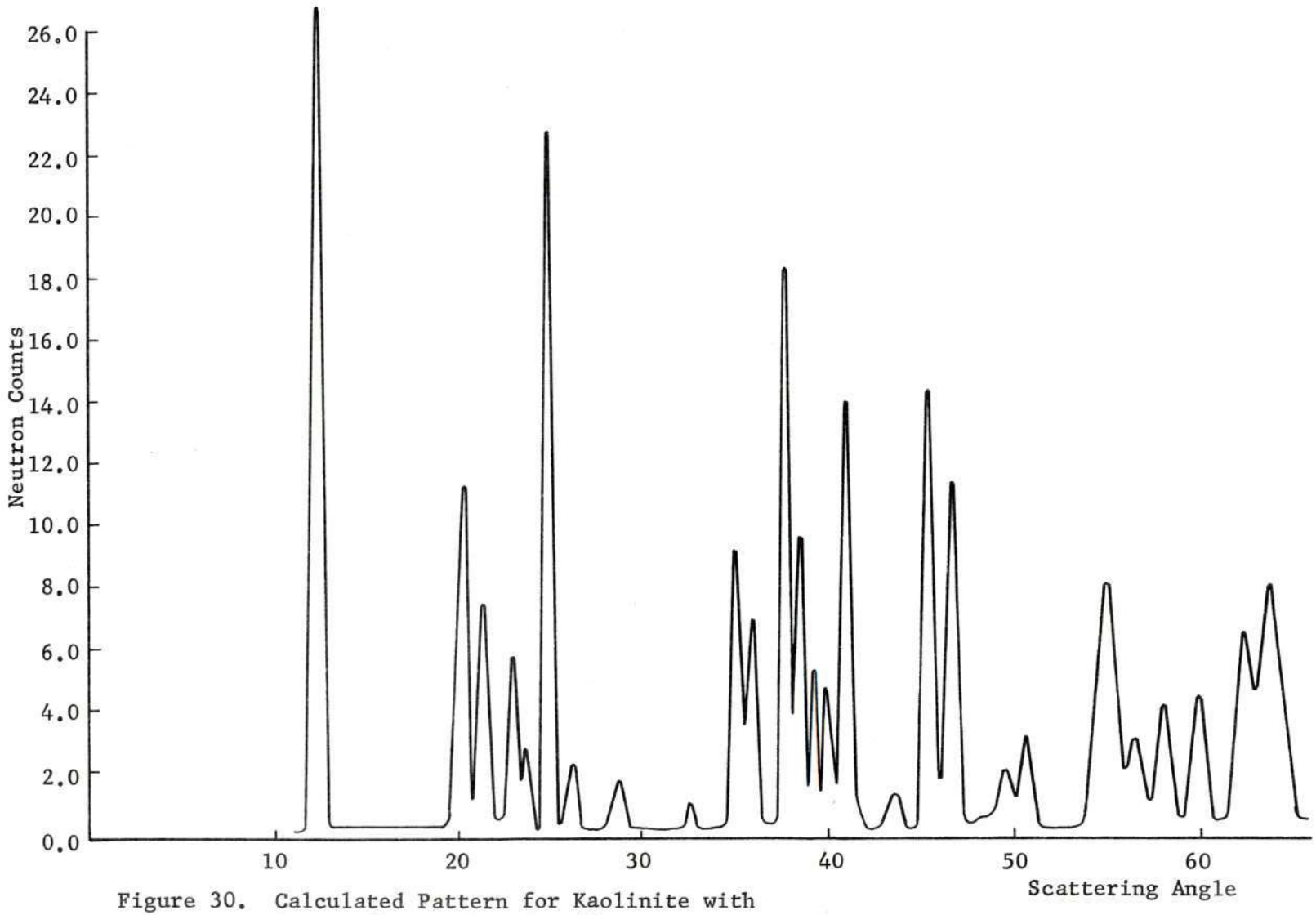

Figure 30. Calculated Pattern for Kaolinite with Proposed Deuterium Coordinates

CHAPTER IV

CONCLUSIONS

1. Differential thermal analysis, thermogravimetric analysis, x-ray diffraction, and electron microscopy indicated that deuterated kaolinite possessed characteristics similar to kaolinite.

2. The examination of the diffuse background of the neutron diffraction pattern indicated that only 7 percent sample hydrogen remained after hydrothermal deuteration.

3. Hydrothermal deuteration did not produce major structural modifications within the unit cell but resulted in the development of a high probability of nb/3 layer shifts between adjacent unit cells.

4. Deuterium coordinates in deuterated kaolinite did not occupy the same coordinates as hydrogen in kaolinite and were found to be:

D_1	.595	.000	.770
D_2	.095	.167	.770
D_3	.595	.333	.770
D_4	.543	.481	.150

5. OD_1, OD_2, and OD_3 bond orientations were inclined away from the c-axis pointing away from aluminum octahedrons and OD_4 pointed down parallel to the c-axis in the vacant octahedral position within the Si-O tetrahedron net.

6. OD bond lengths in deuterated kaolinite were longer than OH bond lengths in kaolinite.

CHAPTER V

RECOMMENDATIONS

Neutron powder diffraction has provided valuable information on the location of hydrogen atoms and the structural consequences of the hydrothermal deuteration of kaolinite. The investigation has proceeded to the point where more structural refinement of deuterated kaolinite and kaolinite is required. Such refinement must include a least squares analysis which would ultimately permit a closer comparison of the structures of kaolinite and deuterated kaolinite leading to more substantial conclusions. A neutron powder diffraction analysis and characterization should also be made of meta kaolinite reconstituted with water. This would confirm the changes in hydrogen positions and indicate whether the change was due to reconstitution or related to the substitution of deuterium. Concurrently with this analysis, the effect of varying time, temperature, and pressure of hydrothermal conditions could be observed in relation to structural reorganization. Insight as to the effects of hydrothermal treatment could also be obtained from analysis of deuterated and undeuterated dickite where x-ray single crystal analysis has proposed hydrogen coordinates.

Similar neutron diffraction analyses could be done on other kaolin group minerals and their deuterated counterparts to provide more valuable information on the clay structures and to give insight on the reason for incomplete reconstitution.

APPENDIX A

MODEL COORDINATES

Table 10. Basic Non-Deuterium Atomic Coordinates

Atom	x	y	z
O_3	.500	.000	.000
O_4	.755	.745	.000
O_5	.245	.745	.000
Si_1	.518	.830	.075
Si_2	.518	.170	.075
O_1	.572	.170	.300
O_2	.572	.830	.300
OH_4	.543	.481	.300
Al_1	.729	.997	.452
Al_2	.229	.834	.453
OH_3	.443	.993	.595
OH_2	.923	.840	.593
OH_1	.425	.670	.591

Table 11. Deuterium Coordinates Used for Proposed Kaolinite Models

Atom	x	y	z
Coordinates for Sanders' Model			
D_1	.461	.000	.723
D_2	.639	.793	.723
D_3	.610	.708	.723
D_4	.543	.481	.165
Coordinates for Brindley and Robinson Model			
D_1	.461	.000	.723
D_2	.639	.793	.723
D_3	.610	.708	.723
D_4	.543	.481	.165
Coordinates for Drits and Kashaev Model			
D_1	.461	.000	.723
D_2	.639	.793	.723
D_3	.610	.708	.723
D_4	.543	.481	.165

Table 12. Initial Hemispherical Variations of Deuterium Positions

Atom	x	y	z
	D_4 Pointing Up		
D_1	.461	.000	.723
D_2	.639	.793	.723
D_3	.610	.708	.723
D_4	.543	.481	.465
	D_1, D_2, and D_3 Pointing Down		
D_1	.461	.000	.465
D_2	.639	.793	.465
D_3	.610	.708	.465
D_4	.543	.481	.165
	D_1 Pointing Down		
D_1	.461	.000	.465
D_2	.639	.793	.723
D_3	.610	.708	.723
D_4	.543	.481	.165
	D_2 Pointing Down		
D_1	.461	.000	.723
D_2	.639	.793	.465
D_3	.610	.708	.723

Table 12. (Concluded)

Atom	x	y	z
D_4	.543	.481	.165
	D_3 Pointing Down		
D_1	.461	.000	.723
D_2	.639	.793	.723
D_3	.610	.708	.465
D_4	.543	.481	.165
	D_1, D_2, and D_3 Random		
D_1	.461	.000	.592
D_2	.639	.793	.592
D_3	.610	.708	.592
D_4	.543	.481	.165
	D_4 Random		
D_1	.461	.000	.723
D_2	.639	.793	.723
D_3	.610	.708	.723
D_4	.543	.481	.300

Table 13. Bond Orientation Variations to Change Deuterium Coordinates

Atom	x	y	z
OD_1, OD_2, OD_3, and OD_4 Perpendicular to the ab-Plane			
D_1	.459	.996	.759
D_2	.959	.843	.759
D_3	.461	.673	.759
D_4	.507	.478	.165
OD_1, OD_2, and OD_3, near Parallel to the c-axis			
D_1	.525	.000	.759
D_2	.025	.167	.759
D_3	.525	.333	.759
D_4	.543	.481	.165
OD_1, OD_2, and OD_3 in Intermediate Positions			
D_1	.595	.000	.759
D_2	.095	.167	.759
D_3	.595	.333	.759
D_4	.543	.481	.165
OD_1, OD_2, OD_3, and OD_4 Parallel to the c-axis			
D_1	.423	.993	.759
D_2	.425	.670	.759
D_3	.833	.870	.759

Table 13. (Continued)

Atom	x	y	z
D_4	.543	.481	.165
OD_1, OD_2, and OD_3 Perpendicular to the c-axis			
D_1	.703	.000	.667
D_2	.214	.167	.667
D_3	.703	.333	.667
D_4	.543	.481	.165
OD_1, OD_2, and OD_3 Point Toward Nearest Neighboring Oxygens			
D_1	.461	.000	.723
D_2	.649	.793	.723
D_3	.590	.708	.723
D_4	.543	.481	.165
OD_1, OD_2, and OD_3 Point Toward Farthest Neighboring Oxygens			
D_1	.461	.997	.789
D_2	.435	.707	.789
D_3	.841	.792	.789
D_4	.543	.481	.165
OD_4 Pointed Straight Down			
D_1	.667	.000	.759
D_2	.167	.167	.759
D_3	.667	.333	.759
D_4	.507	.478	.165

Table 13. (Continued)

Atom	x	y	z
OD_4 Pointed Diagonally Away from c-axis			
D_1	.667	.000	.759
D_2	.167	.167	.759
D_3	.667	.333	.759
D_4	.742	.481	.242
OD_4 Directed Diagonally Toward the c-axis			
D_1	.667	.000	.759
D_2	.167	.167	.759
D_3	.667	.333	.759
D_4	.334	.481	.180
D_4 Directed Toward Basal O_3			
D_1	.667	.000	.759
D_2	.167	.167	.759
D_3	.667	.333	.759
D_4	.522	.740	.150
D_4 Directed Toward Basal O_5			
D_1	.667	.000	.759
D_2	.167	.167	.759
D_3	.667	.333	.759
D_4	.644	.613	.150

Table 13. (Concluded)

Atom	x	y	z
	D_4 Directed Toward Basal O_4		
D_1	.667	.000	.759
D_2	.167	.167	.759
D_3	.667	.333	.759
D_4	.394	.613	.150

Table 14. Z-axis Displacement Variations for Deuteriums

Atom	x	y	z
	OD_1, OD_2, and OD_3 Lengthened		
D_1	.667	.000	.789
D_2	.167	.167	.789
D_3	.667	.333	.789
D_4	.543	.481	.165
	OD_1, OD_2, and OD_3 Shortened		
D_1	.667	.000	.700
D_2	.167	.167	.700
D_3	.667	.333	.700
D_4	.543	.481	.165
	OD_4 Lengthened		
D_1	.667	.000	.759
D_2	.167	.167	.759
D_3	.667	.333	.759
D_4	.543	.481	.150
	OD_4 Shortened		
D_1	.667	.000	.759
D_2	.167	.167	.759
D_3	.667	.333	.759
D_4	.543	.481	.180

Table 15. Coincidence of Deuteriums with Hydrogens in Various Projections

Atom	x	y	z
	D_1 with H_1 in the (010) Projection		
D_1	.461	.000	.759
D_2	.167	.167	.759
D_3	.667	.333	.759
D_4	.543	.481	.165
	D_3 with H_3 in the (010) Projection		
D_1	.667	.000	.759
D_2	.167	.167	.759
D_3	.139	.333	.759
D_4	.543	.481	.165
	D_2 with H_2 in the (010) Projection		
D_1	.667	.000	.759
D_2	.167	.110	.759
D_3	.667	.333	.759
D_4	.543	.481	.165
	D_2, D_3 with H_2, H_3 in the (100) Projection		
D_1	.667	.000	.759
D_2	.167	.208	.759

Table 15. (Concluded)

Atom	x	y	z
D_3	.667	.293	.759
D_4	.543	.481	.165
D_1, D_2, and D_3 Parallel to the c-axis in the (100) Projection			
D_1	.667	.000	.759
D_2	.167	.170	.759
D_3	.667	.340	.759
D_4	.543	.481	.165
D_2, D_3 Directed Toward D_1 in the (100) Projection			
D_1	.667	.000	.759
D_2	.167	.110	.759
D_3	.667	.463	.759
D_4	.543	.481	.165

Table 16. Structural Changes Within the Deuterated Kaolinite Unit Cell

Atom	x	y	z
Rotation of Silica Tetrahedrons			
2.5°			
O_3	.500	.000	.000
O_4	.764	.761	.000
O_5	.275	.748	.000
Si_1	.505	.170	.075
Si_2	.505	.830	.075
O_1	.560	.170	.300
O_2	.560	.830	.300
5.0°			
O_3	.500	.000	.000
O_4	.784	.767	.000
O_5	.293	.741	.000
Si_1	.492	.169	.075
Si_2	.492	.831	.075
O_1	.541	.169	.300
O_2	.541	.831	.300
Statistical Distribution in Octahedral Sites			
Al_1	.729	.997	.452
Al_2	.229	.834	.453
Al_3	.729	.666	.452

Table 16. (Concluded)

Atom	x	y	z
	Octahedral Super-Position		
Well Crystallized Kaolinite			
Al_1	.729	.997	.452
Al_2	.229	.834	.453
Slightly Distorted Kaolinite			
Al_1	.729	.997	.452
Al_2	.229	.166	.452
Fireclay Kaolinite			
Al_1	.229	.166	.452
Al_2	.229	.834	.452
	Basal Plane Puckering		
O_3	.500	.000	.000
O_4	.755	.745	.027
O_5	.245	.745	.027

APPENDIX B

NEUTRON DIFFRACTION DATA

Table 17. Neutron Diffraction Data

	Intensity in Tenth Degree Intervals									
2θ	.0	.1	.2	.3	.4	.5	.6	.7	.8	.9
9.0		843	810	756	782	810	798	805	811	803
10.0	793	761	794	756	760	749	731	709	788	745
11.0	781	781	815	817	896	890	947	1056	1133	1154
12.0	1026	957	865	843	750	750	737	728	711	757
13.0	703	644	692	694	690	704	685	685	704	684
14.0	675	701	701	684	723	707	752	683	711	691
15.0	716	695	659	663	666	679	682	673	660	706
16.0	712	655	688	689	684	669	715	741	783	912
17.0	901	995	1089	983	863	822	710	704	743	740
18.0	775	819	813	852	898	927	912	902	872	750
19.0	801	734	708	815	834	921	931	865	949	910
20.0	920	934	806	729	815	781	835	776	764	825
21.0	814	885	816	788	820	867	827	880	853	886
22.0	826	859	791	783	813	792	800	860	800	852
23.0	798	814	798	859	829	759	853	816	861	890
24.0	879	815	860	860	785	828	803	783	750	778
25.0	817	870	930	1007	1040	951	874	832	779	771
26.0	747	761	804	806	878	951	888	919	838	865
27.0	845	849	775	792	737	780	755	764	737	717
28.0	694	723	696	728	741	735	745	746	759	745

Table 17. (Continued)

	Intensity in Tenth Degree Intervals									
2θ	.0	.1	.2	.3	.4	.5	.6	.7	.8	.9
29.0	764	646	705	652	767	821	794	763	696	691
30.0	698	646	714	707	687	642	685	648	690	645
31.0	699	622	662	673	705	683	664	676	694	705
32.0	668	738	713	646	661	675	686	668	674	661
33.0	677	669	678	792	727	701	644	728	673	702
34.0	716	713	842	993	1221	1411	1514	1669	1829	2233
35.0	2647	3099	3600	4197	4365	4098	3236	2310	1714	1330
36.0	1016	959	996	1014	939	979	975	943	1057	1206
37.0	1432	1842	2166	2155	1935	1658	1590	1754	2145	2720
38.0	3208	3192	2818	2507	2015	1814	1602	1505	1399	1272
39.0	1012	1001	886	841	828	837	869	865	1012	1166
40.0	1200	1243	1172	1177	1169	1178	1123	1072	1088	1009
41.0	885	896	840	859	828	859	882	866	873	787
42.0	827	740	751	732	757	782	767	768	743	667
43.0	710	693	751	748	753	696	740	722	767	740
44.0	860	899	943	900	865	926	922	1016	1101	1238
45.0	1328	1356	1371	1440	1237	1227	1111	1038	993	938
46.0	970	941	900	933	832	840	798	733	745	726
47.0	755	759	788	813	763	768	819	739	801	749
48.0	759	766	745	780	809	818	860	840	809	746

Table 17. (Concluded)

	Intensity in Tenth Degree Intervals									
2θ	.0	.1	.2	.3	.4	.5	.6	.7	.8	.9
49.0	839	720	693	752	692	682	688	687	724	733
50.0	726	715	766	818	852	878	901	801	779	720
51.0	683	672	659	692	612	611	657	603	634	612
52.0	626	594	589	629	635	650	688	639	666	667
53.0	683	727	673	735	764	766	816	962	942	901
54.0	981	923	884	860	884	881	933	905	950	858
55.0	897	877	835	843	834	830	818	830	871	800
56.0	826	790	824	788	771	795	773	767	809	764
57.0	775	724	774	771	770	813	795	789	805	761
58.0	813	778	832	878	840	910	893	943	939	1038
59.0	953	917	983	894	864	855	830	781	814	732
60.0	784	726	749	697	759	722	715	734	838	851
61.0	963	1162	1397	1565	1804	1952	2006	1922	1843	1622
62.0	1357	1110	1042	925	892	917	942	1014	985	978
63.0	997	1040	1014	932	879	939	920	870	854	890
64.0	825	854	897	868	829	898	865	908	833	811
65.0	757	787	747	728	840	773	763	809	764	826
66.0	852	777	832	825	868	806	852	819	841	826
67.0	854	804	844	883	897	869	864	790	848	858
68.0	812	813	819	842	759	819	770	780	767	740
69.0	748	765	789	801	771	867	757	803	793	740
70.0	768									

BIBLIOGRAPHY*

1. Roy, R., and Brindley, G. W. "A Study of the Hydrothermal Reconstitution of the Kaolin Minerals," Clay and Clay Minerals, 125-132, 1956.

2. Serratosa, J. M., Hidalgo, J. M., and Vinas, J. M., "Orientation of OH Bonds in Kaolinite," Nature, 486-487, 1962.

3. Newnham, R. E., "Crystal Structure of the Mineral Dickite," Ph.D. Thesis, Pennsylvania State University, 1956.

4. Ledoux, R. L., "Infrared Studies of the Hydroxyl Groups in Intercalated Kaolinite Complexs," Thirteenth National Conference on Clays and Clay Minerals, 13, 289-315, 1966.

5. Sanders, T. H. B., "Neutron Diffraction Investigation of Well Crystallized Kaolinite," M.S. Thesis, Georgia Institute of Technology, 1970.

6. Brindley, G. W. and Robinson, K., "The Structure of Kaolinite," Mineral Mag., 27, 242-253, 1946.

7. Gruner, J. W., "The Structure of the Chlorites," Proc. Nat. Acad. Sci., 16, 578, 1930.

8. Zvyagin, B. B., "Electron-diffraction Determination of the Structure of Kaolinite," Kristallografiya, 5, 40-50, 1960.

9. Drits, V. A. and Kashaev, A.A., "An X-ray Study of a Single Crystal of Kaolinite," Kristallografiya, 5, 207-210, 1960.

10. Newnham, R. E., "A Refinement of the Dickite Structure and Some Remarks on Polymorphism of Kaolin Minerals," Mineral Mag., 32, 683-704, 1961.

11. Klug, H. P. and Alexander, L. E., "X-ray Diffraction Procedures," John Wiley and Sons, Inc., New York, 1959.

*Abbreviations follow the form used by Chemical Abstracts (1965).

BIBLIOGRAPHY (Concluded)

12. Harris, B. B., "Investigation of Hydrogen and its Role in Dehydration Processes in Halloysite," M.S. Thesis, Georgia Institute of Technology, 1971.

13. Blech, I. A., and Averbach, B. L., "Multiple Scattering of Neutrons in Vanadium and Copper," Phys. Rev., 137, A1113-A1116, 1965.

14. Bacon, G. E., "Neutron Diffraction," Monographs on the Physics and Chemistry of Materials, Oxford University Press, London, 1962.

15. Caglioti, G., Paoletti, A. and Ricci, F. P., "Choice of Collimators for a Crystal Spectrometer for Neutron Diffraction," Nuclear Instrum., 3, 223-229, 1958.

16. Wilson, A. J. C., "X-ray Optics," Methuen and Co., London, 1962.